Characteristics, sources, and reactions of nitrous acid during winter at an urban site in the Central Plains Economic Region in China

Qi Hao[1,3], Nan Jiang[2,3]*, Ruiqin Zhang[2,3], Liuming Yang[1,3], and Shengli Li[2,3]

[1] College of Chemistry, Zhengzhou University, Zhengzhou 450001, China

[2] School of Ecology and Environment, Zhengzhou University, Zhengzhou 450001, China

[3] Research Institute of Environmental Science, Zhengzhou University, Zhengzhou 450001, China

Abstract

Nitrous acid (HONO) in the core city of the Central Plains Economic Region was measured using an ambient ion monitor from January 9 to 31, 2019. Measurement time intervals were classified into the following periods in accordance with the daily mean values of $PM_{2.5}$: clean days (CD), polluted days (PD), and severely polluted days (SPD). The HONO concentrations during CD, PD, and SPD were 1.2, 2.3, and 3.7 ppbv, respectively. The contribution of the homogeneous reaction, heterogeneous conversion, and direct emission to HONO sources varied under different pollution levels. The mean values of the net HONO production of the homogeneous reaction (P^{net}_{OH+NO}) in CD, PD, and SPD periods were 0.13, 0.26, and 0.56 ppbv h^{-1}, respectively. The average conversions of NO_2 (C_{HONO}) in CD, PD, and SPD periods were 0.72×10^{-2}, 0.64×10^{-2}, and 1.54×10^{-2} h^{-1}, respectively, indicating that the heterogeneous conversion of NO_2 was unimportant than the homogeneous reaction. Furthermore, the net production of the homogeneous reaction may have been the main factor for the increase in HONO under high-NO_X conditions (i.e., when the concentration of NO was higher than that of NO_2) at nighttime. Daytime HONO budget analysis showed that the mean values of the unknown source ($P_{unknown}$) during CD, PD, and SPD periods were 0.26, 0.40, and 1.83 ppbv h^{-1}, respectively. The values of P^{net}_{OH+NO}, C_{HONO}, and $P_{unknown}$ in the SPD period were comparatively larger than those in other periods, indicating that HONO participated in many reactions. The proportions of nighttime HONO sources also changed during the entire sampling period. Direct emission and a

heterogeneous reaction controlled HONO production in the first half of the night and provided a contribution larger than that of the homogeneous reaction. The proportion of homogenization gradually increased in the second half of the night due to the steady increase in NO concentration. The hourly level of HONO abatement pathways, except for OH + HONO, was at least 0.22 ppbv h^{-1} in the SPD period. The cumulative frequency distribution of the $HONO_{emission}$/HONO ratio (less than 20%) was approximately 77%, which suggested that direct emission was not important. The heterogeneous HONO production increased when the relative humidity (RH) increased, but it decreased when RH increased further. The average HONO/NO_X ratio (4.9%) was more than twice the assumed globally averaged value (2.0%).

1. Introduction

Nitrous acid (HONO) is important in the photochemical cycle and can provide hydroxyl radicals (OH) (Harrison et al., 1996):

$$HONO + h\nu \rightarrow \cdot OH + NO \quad (300\ nm < \lambda < 405\ nm) \qquad (R1).$$

According to measurement and simulation studies (Alicke et al., 2002), the contribution of HONO to ·OH concentration can reach 25−50%, especially when the concentration of OH radicals produced by the photolysis of ozone, acetone, and formaldehyde is relatively low (two to three hours after sunrise) (Czader et al., 2012). HONO photolysis was the most important primary source of ·OH which contributed up to 46 % of the total primary production rate of radicals for daytime conditions (Tan et al., 2018). ·OH is an important oxidant in the atmosphere, and it can react with organic substances, control the oxidation capacity of the atmosphere, and accelerate the formation of secondary aerosols in the urban atmosphere (Sörgel et al., 2011). Therefore, the changes in the contribution of the homogeneous reaction, heterogeneous conversion, and direct emission during pollution can be observed by studying the formation mechanism of HONO.

Several instruments have been used to determine ambient HONO concentrations, and these include differential optical absorption spectrophotometer (DOAS)

(Elshorbany et al., 2012; Winer and Biermann, 1994), long path absorption photometer (LOPAP) (Heland et al., 2001), wet chemical derivatization technique-HPLC/UV-Vis detection (Michoud et al., 2014), stripping coil-UV/Vis absorption photometer (SC-AP) (Pinto et al., 2014), IBBCEAS (Duan et al., 2018; Min et al., 2016), CIMS (Hirokawa et al., 2009; Roberts et al., 2010), and ambient ion monitor (AIM) (VandenBoer et al., 2014). A result comparison of different instruments showed that SC-AP is compatible with two spectral measurement instruments, namely, LOPAP and DOAS (Pinto et al., 2014). Compared with HONO measured by SC-AP deployed onsite, HONO measured by AIM has a small error and is within the acceptable analytical uncertainty (VandenBoer et al., 2014). Previous studies have reported that HONO concentrations range from a few pptv in clean remote areas to several ppbv (0.1−2.1 ppbv) in air-polluted urban areas (Hou et al., 2016; Michoud et al., 2014).

The sources of HONO are direct emission and homogeneous and heterogeneous reactions (Acker et al., 2005; Grassian, 2001; Kurtenbach et al., 2001). HONO can be directly discharged into the atmosphere during vehicle operation and biomass combustion. Through a tunneling experiment, Kurtenbach et al. (2001) have discovered that motor vehicles emit a small amount of HONO, and the HONO/NO_X ratio of HONO combustion sources (aside from NO_X and other pollutants) is 0.1–0.8%. Another study showed that the homogeneous reaction of NO and OH radicals is the major source of HONO under increased NO concentrations (Spataro et al., 2013). Furthermore, HONO can react with the ·OH (Alicke et al., 2003; Vogel et al., 2003). Tong et al. (2015) used NO + OH and HONO + OH homogeneous reactions, to calculate the net generation rate of HONO homogeneous reactions at night, which are expressed as:

$NO + {\cdot}OH \rightarrow HONO$ (R2);

$HONO + {\cdot}OH \rightarrow NO_2 + H_2O$ (R3).

Such calculations have been applied in studies on homogeneous reactions and daytime budgets (Hou et al., 2016; Huang et al., 2017). These are studies of homogeneous reactions, and some researchers have begun to explore the mechanism of NO_2

heterogeneous reactions. Finlayson-Pitts et al. (2003) studied the mechanism of chemical adsorption of NO_2 and H ions on the adsorbed surface was revealed by using isotope-labeled water:

$$2NO_2 + H_2O \rightarrow HONO + HNO_3 \quad \text{(R4)}.$$

In China, most studies for HONO have been focused on the Yangtze River Delta, Pearl River Delta, and Jing-Jin-Ji region. For example, Hao et al. (2006) reported that field measurement results, especially HONO/NO_2 and relative humidity (RH), have a significant correlation and proved that heterogeneous reactions are an important source of nighttime HONO. Although the specific chemical mechanisms of heterogeneous reactions remain unknown, the intensity of HONO formation by NO_2 can be expressed by the HONO conversion frequency (Alicke et al., 2002; Li et al., 2012). Su et al. (2008a) revealed the importance of the ·OH from HONO during daytime (9:00–15:00 local time) and found that many unknown sources which are closely related to the solar radiation leading to HONO formation. The unknown sources of HONO may include the NO_2 photolysis of sooty surface and adsorbed nitric acid and nitrate at UV wavelengths (Kleffmann et al., 1999). The homogeneous nucleation of NO_2, H_2O, and NH_3 is the HONO formation pathway (Zhang and Tao, 2010). In the meanwhile, HONO can deposit and react with amines in forming nitrosamines (Li et al., 2012) for sinking. The method of budget analysis needs to include the HONO sources and sinks. The researchers suggested that the method of budget analysis is crucial for obtaining the missing source. Spataro et al. (2013) measured the HONO level in Beijing's urban area and discussed the spatiotemporal changes, meteorological effects, and contributions of HONO from different sources. They used the measured HONO data to compare pollution periods in Beijing's urban and suburban areas. Tong et al. (2015) discovered that the pathway of the HONO formation mechanism, namely, direct emission, heterogeneous formation, and homogeneous reaction is the same, but the pathway is different in the two sites. A few studies (Cui et al., 2018; Hou et al., 2016) compared the characteristics and sources of HONO during severe-pollution and clean periods.

Although the definitions of the two periods are different, both can be used to analyze the diurnal variation, source, and daytime budget of HONO during the aggravation of pollution.

There is no study of HONO in the Central Plains Economic Region (CPER), with a total population of 0.18 billion by the end of 2011. CPER is the important region for food production and modern agriculture published by the Chinese government (http://www.gov.cn/zhengce/content/2011-10/07/content_8208.htm). The file described the different factors which affect atmospheric pollution, including the level of economic development, energy structure, industrial structure and geographical location (solar radiation) with the Yangtze River Delta, Pearl River Delta, and Jing-Jin-Ji region. As the core city of CPER, Zhengzhou characterized by severe PM (particulate matters) pollution (Jiang et al., 2017; 2018d), is selected in the study. In recent years, comprehensive PM research has been conducted on the chemical characteristics of PM in Zhengzhou (Jiang et al., 2018b; Li et al., 2019), source apportionment (Jiang et al., 2018c; 2018e; Liu et al., 2019), health risks (Jiang et al., 2019a; 2019b), and emission source profiles (Dong et al., 2019; Jiang et al., 2018a). However, no study has been performed on the sources and characteristics of HONO in Zhengzhou. Moreover, no synthetic research on different pollution levels in the area is available. In the current study, AIM was used to sample and analyze HONO concentrations. The interactions between HONO and other factors, such as $PM_{2.5}$, during pollution, were assessed to understand the formation and removal of HONO and the influence on different pollution periods. The levels of $PM_{2.5}$ were divided into three periods to analyze the HONO sources, sinks, and reactions in different periods. Many papers (Huang et al., 2017; Tong et al., 2016) took $PM_{2.5}$ as the main control factor of HONO, and studied the differences of HONO sources and characteristics between clean and polluted periods. No homogeneous reaction, direct emission, heterogeneous reaction, and daytime budget analysis were conducted during the period of worsening pollution (namely HD period in this paper). Total NO_X emissions in cities with different leading factors of emissions have been declining year

by year due to Chinese government emission control measures, but some Chinese cities are still in high-NO_X areas (e.g. Beijing, Shanghai, Guangzhou and Zhengzhou.) (Kim et al., 2015; Liu et al., 2017). Under high-NO_X conditions, some papers (Cui et al., 2018; Hou et al., 2016) suggested that heterogeneous reaction was the main source of HONO and did not conduct a quantitative analysis of homogeneous reaction, especially in winter. So, we explore relevant studies of homogeneous reactions. In addition, the source contributions of HONO at night varied with the degree of pollution level were not explained. RH was also analyzed to provid a detailed understanding of HONO generation intensity under different RH conditions. Analysis of the sources of HONO at night provides strong support for conducting HONO budget analysis during daytime. To the best of the authors' knowledge, the formation characteristics of HONO at continuous and high time resolutions and different pollution levels have not been studied in Zhengzhou. This work can assist the governments of the CPER in formulating policy to decrease the level of HONO precursors, i.e., NO and NO_2, and HONO direct emission from the vehicle.

2. Experiment and methods

2.1. Sampling site and period

The sampling site is on the rooftop (sixth floor) of a building in Zhengzhou University (34°48' N, 113°31' E), which is located in the northwestern part of Zhengzhou, China. The observation height is about 20 m from the ground, and the observation platform is relatively open without any tall buildings around. The site is about 500 m from the western Fourth-Ring Expressway of Zhengzhou City and about 2 km from Lian Huo Expressway to the north. The measurement period was from January 9 to 31, 2019. Daily data were divided into two periods, namely, daytime (7:00–18:00 local time) and nighttime (19:00–6:00 the next day, LT).

2.2. Instruments

AIM (URG-9000D, Thermo, USA), an online ion chromatographic monitoring system for particle and gas components in the atmosphere, was used to measure HONO

concentration continuously at a temporal resolution of 1 h. The atmospheric airflow entered the $PM_{2.5}$ cyclone cutting head through the sample tube, and gas–solid separation was performed with a parallel plate denuder with a new synthetic polyamide membrane. The denuder had no moving parts and could be changed without stopping the sampler. HONO was absorbed by the denuder with an absorption liquid (5.5 mol m^{-3} H_2O_2). The chemicals that could be oxidized were absorbed by H_2O_2 on the porous membrane surface, but several gases (e.g., O_2 and N_2) were expelled by the air pump. The abundance of other gaseous acids and bases affected the efficiency of HONO collection by AIM due to the relation between Henry's law constant and pH. This measurement method and its details have been successfully evaluated in many field studies (Markovic et al., 2012; Wang et al., 2019; Yang et al., 2020), and shown in the supplement. In addition, a QXZ1.0 automatic weather station (Yigu Technologies, China) was used for synchronous observation of meteorological parameters, including temperature (T), RH, wind direction (WD), and wind speed (WS). The temporal resolution of the model analyzer (TE [used for measuring O_3], 48i [used for measuring CO], 42i [used for measuring NO, NO_X, and NO_2], and TEOM 1405 $PM_{2.5}$ monitor [used for measuring $PM_{2.5}$], Thermo Electron, USA) is 1 h. Detailed information can be found in the work of (Wang et al., 2019). Measurement technique, detection limit, and accuracy of measured species are shown in **Table S1**.

During the sampling period, all instruments were subject to strict quality control to avoid possible contamination. The instrument accessories and sampling process were periodically replaced and calibrated, respectively. The instrument parts and consumables were changed before the observation process, and the sampling flow was calibrated to reduce the negative effect of accessories. Before this measurement period, the membrane of the denuder has been replaced and standard anion and cation solutions have been prepared on Jan. 3rd. The standard curve should be drawn to ensure the appropriateness of the correlation coefficient ($\geqslant$ 0.999) and the accuracy of the sample retention time and response value. The minimum detection limit of AIM was 0.004

ppbv. Other detailed information can be found in the work of (Wang et al., 2019).

3. Results and Discussion

3.1. Temporal variations of meteorological parameters and pollutants

The daily changes in meteorological parameters and $PM_{2.5}$ are shown in **Fig. 1**. In accordance with the daily average concentration level of $PM_{2.5}$, the analysis and measurement process was divided into three periods (clean days [CD], polluted days [PD], and severely polluted days [SPD]). The days wherein the daily averages of $PM_{2.5}$ were lower than the daily average of second grade in China National Ambient Air Quality Standards (CNAAQS) (75 μg m^{-3}) represented CD (January 9, 16, 17, 21, 22, 23, 26, and 31), with RH ranging from 5 to 79% and WS ranging from 0 to 4.2 m s^{-1}. The days wherein the daily averages of $PM_{2.5}$ were between 75 and 115 μg m^{-3} represented PD (January 10, 15, 18, 20, 25, 27, and 28), with RH ranging from 17 to 86% and WS ranging from 0 to 4.6 m s^{-1}. The days wherein the daily averages of $PM_{2.5}$ were higher than 115 μg m^{-3} represented SPD (January 11, 12, 13, 14, 19, 24, 29 and 30), with RH ranging from 30 to 96% and WS ranging from 0 to 3.5 m s^{-1}. Northwest or east wind was observed in most of the observation periods, except for January 21–22. WD was north, the maximum WS reached 4 m/s, the $PM_{2.5}$ concentration decreased rapidly, and the effect of pollutant removal was evident. **Table 1** lists the data statistics of HONO, $PM_{2.5}$, NO_2, NO, NO_X, HONO/NO_2, HONO/NO_X, O_3, CO, T, RH, WS, and WD during the measurement period together with their mean value ± standard deviation. The meteorological parameters in **Table 1** show that the average RH in CD, PD, and SPD periods was 33, 49, and 68%, respectively. In SPD, RH was high and WD was low (mean value of 0.4 m s^{-1}).

In accordance with the data on trace gases, the average HONO values in CD, PD, and SPD were 1.1, 2.3, and 3.7 ppbv, respectively. The mean values of NO_2 were 25, 33, and 42 ppbv (46, 63, and 78 μg m^{-3} lower than the first grade in CNAAQS [80 μg m^{-3}]), respectively. The mean values of CO were 1, 1, and 2 ppmv (1, 2, and 2 mg m^{-3} lower than the first grade in CNAAQS [4 mg m^{-3}]), respectively. **Fig. 2** shows the

concentration changes in HONO and gas species throughout the measurement period. The variations of the average HONO, $PM_{2.5}$, NO_2, and CO in the three periods were similar. The mean values of all pollutant concentrations except O_3 in the SPD period were the largest, and those in the CD period were the smallest. The highest mean value of O_3 occurred in the CD period, similar to previous observations (Hou et al., 2016; Huang et al., 2017; Zhang et al., 2019).

The HONO concentrations ranged from 0.2 to 14.8 ppbv and had an average of 2.5 ppbv, which is higher than the average values of 0.6 (Rappenglück et al., 2013), 1.5 (Hou et al., 2016), and 1.0 ppbv (Huang et al., 2017) in previous urban studies. The diurnal variations of HONO during the measurement were similar in the three periods, as shown in **Fig. 3** and **Fig. 4**. The diurnal variations of HONO, NO, NO_2, O_3, $HONO/NO_2$, and $HONO/NO_X$ are illustrated in **Fig. 4**. The error bars of **Fig. 4** were placed separately in the tables of the supplement (**Table S2**). After sunset, the HONO concentrations in CD, PD, and SPD began to accumulate due to the attenuation of solar radiation and the stabilization of the boundary layer (Cui et al., 2018). The maximum values of 1.7, 4.1, and 6.9 ppbv were reached in the morning (08:00–10:00 LT) in CD, PD, and SPD, respectively. After 10:00 LT, the HONO concentration decreased because of the increased solubility and rapid photolysis, remaining at a low level before sunset (14:00–16:00 LT). The NO concentration decreased rapidly in the forenoon, and remained low in the afternoon. After sunset, the concentrations of NO and NO_2 began to increase and remained at a higher level than the daytime. Furthermore, the diurnal variation of NO in the CD period was similar to that of NO_2. The peak was reached at around 09:00 LT due to vehicle emission in the morning rush hours, and the lowest value was observed at around 16:00 LT. After 18:00 LT, the boundary layer height decreased in the evening rush hours, resulting in an increase in NO and NO_2 concentrations (Hendrick et al., 2014). O_3 showed a diurnal cycle and had maximum values in CD, PD, and SPD periods in the afternoon. The $HONO/NO_2$ ratio is commonly used to estimate the formation of HONO in NO_2 transformation (Wang et

al., 2013). Compared with HONO formation, NO_2 transformation is less affected by the migration of atmospheric airmass during atmospheric migration (Li et al., 2012). The HONO/NO_2 ratio in the CD period began to increase after sunset and reached its peak at night. Then, it decreased in the morning as a result of the enhancement of NO_2 emission and photolysis of HONO. However, the mean value of HONO/NO_2 in PD and SPD periods gradually increased from nighttime and eventually reached the maximum values of 14.3 and 18.9% at 09:00 and 10:00 LT, respectively. The average HONO/NO_X ratio (4.9%) was more than twice the assumed globally averaged value (2.0%) (Elshorbany et al., 2014). This result indicates that the strength of the heterogeneous reaction increased slightly with the exacerbation of pollution. The HONO/NO_2 ratio showed a diurnal cycle with a low level in the afternoon and a high level after sunset due to the heterogeneous reaction of NO_2 on the ground and aerosol surface (Su et al., 2008b). For comparison, the daytime and nighttime HONO, HONO/NO_2, and HONO/NO_X mean values in other cities around the world are listed in **Table 2**. The values of HONO, HONO/NO_2, and HONO/NO_X in Zhengzhou are relatively higher than those in other parts of the world. The reason for this phenomenon is that Zhengzhou is a high-NO_X area which provides HONO with abundant precursors (NO_2 and NO) in winter (Kim et al., 2015).

3.2. Nocturnal HONO sources and formation

3.2.1. Homogeneous reaction of NO and OH

The homogeneous reaction of NO and OH (R2 and R3) is the main pathway of HONO formation in the gas phase. Spataro et al. (2013) found that the formation mechanism leads to an increase in HONO in high-pollution areas with an increase in NO at night. P^{net}_{OH+NO} can be understood as the net hourly HONO production amount of homogeneous reaction and is calculated as

$$P^{net}_{OH+NO} = k_{OH+NO}[OH][NO] - k_{OH+HONO}[OH][HONO] \quad (1).$$

At T = 298 K and P = 101 kPa, the rate constants of k_{OH+NO} and $k_{OH+HONO}$ are 9.8×10^{-12} and 6.0×10^{-12} cm^3 $molecule^{-1}$ s^{-1}, respectively (Atkinson et al., 2004; Sander

et al., 2003). [OH] is the concentration of ·OH that was not measured during the campaign. Tan et al. (2018) found that by the field measurement, the average concentration of ·OH in Beijing at nighttime was about 2.5×10^5 molecule cm^{-3}. Moreover, the same ·OH concentration was also used to calculate the homogeneous reaction of HONO in the recent researches of Beijing (Zhang et al., 2019), Shanghai (Cui et al., 2018), and Xi'an (Huang et al., 2017). And, nighttime OH concentration increased as the latitude decreases ranged 3 to 6×10^5 molecule cm^{-3} (Lelieveld et al., 2016). Zhengzhou has a lower latitude than Beijing, so the concentration of OH used in this study is 2.5×10^5 molecule cm^{-3}. P^{net}_{OH+NO} primarily depends on the concentrations of NO and HONO because the values of k_{OH+NO} and $k_{OH+HONO}$ are close. **Fig. 5** shows the nocturnal variations of P^{net}_{OH+NO}, NO, and HONO during CD, PD, and SPD periods. The uncertainties of P^{net}_{OH+NO}, NO, and HONO in **Fig. 5** are shown in **Table S3**. When the NO levels were high, the variations of P^{net}_{OH+NO} followed those of NO during the three periods (Atkinson et al., 2004). The mean value of P^{net}_{OH+NO} was 0.33 ppbv h^{-1}, and the specific values in CD, PD, and SPD periods were 0.13, 0.26, and 0.56 ppbv h^{-1}, respectively. We assumed $\pm$ 50% ·OH values to estimate the uncertainty of P^{net}_{OH+NO}. The ·OH values of 1.25×10^5 and 3.75×10^5 molecule cm^{-3} were calculated the P^{net}_{OH+NO} values of 0.16 and 0.49 ppbv h^{-1}.

P^{net}_{OH+NO} varied from 0.01 to 0.47 ppbv h^{-1} during the CD period. The mean value of P^{net}_{OH+NO} increased before midnight, decreased after midnight, and increased slightly at 3 am. In the PD period, P^{net}_{OH+NO} ranged from 0.07 to 0.44 ppbv h^{-1}. The situation was similar to that in the CD period, except that the value remained almost constant. In addition, the contribution of HONO from homogeneous reaction during the SPD period was larger than those in the CD and PD periods, and the level of P^{net}_{OH+NO}, with an average value of 0.56 ppbv h^{-1}, was lower than the value in a previous study (2.18 ppbv h^{-1} in Beijing) (Tong et al., 2015). From 19:00 LT to 03:00 LT, the mean value of P^{net}_{OH+NO} increased from 0.15 to 0.9 ppbv h^{-1}. HONO increased from 2.84 to 4.59 ppbv and subsequently decreased to 4.43 ppbv. By integrating P^{net}_{OH+NO} during the eight

hours, the homogeneous reaction can provide an accumulated HONO formation of at least 3.36 ppbv (i.e., 0.15 + 0.20 + 0.25 + 0.25 + 0.35 + 0.56 + 0.7 + 0.9 ppbv). However, the mean accumulation value of measured HONO in this nighttime period was merely 1.59 ppbv. With the increase in pollution level, the HONO accumulation period at nighttime increased. This result indicates that first, the homogeneous reaction of OH + NO is sufficient to augment HONO in the first half of the night, although NO_2 transformation and other sources may still exist. When the concentration of NO is relatively high, the net production generated by OH + NO may be the leading factor for the increase in HONO at night (Tong et al., 2015). Second, the hourly level of HONO abatement pathways, except OH + HONO, should be at least 0.22 ppbv h^{-1} (i.e., 3.36 – 1.59 ppbv)/8 h). This phenomenon may arise because the dry deposition on ground surfaces can be the main HONO removal pathway at night, similar to a previous study (Li et al., 2012).

3.2.2. Direct emission

At present, no HONO emission inventory or emission factor database for Zhengzhou is available. As a result, estimating any HONO from direct emission is difficult. In the current study, directly emitted HONO could have been generated by vehicle exhaust and biomass combustion because the site is close to the western Fourth-Ring Expressway of Zhengzhou City and about Lian Huo Expressway to the north. Hence, only night data (17:00–06:00 LT) were considered to avoid the problem of instant photolysis of directly emitted HONO. In a previous study, the $HONO/NO_X$ ratio from tunnel measurement was set to 0.65% to estimate an upper limit of HONO emitted by traffic near the site (Kurtenbach et al., 2001). The minimum value of $HONO/NO_X$ in the SPD period in the current work was 1.5%, which is slightly higher than the value measured in the abovementioned study. Directly emitted HONO at night was not transformed immediately. The HONO concentrations corrected by direct emissions are given as

$$[HONO]_{correct} = [HONO] - [HONO]_{emission} = [HONO] - 0.0065 \times [NO_X] \quad (2),$$

where $[HONO]_{emission}$, $[NO_X]$, and 0.0065 are direct emission HONO concentration, NO_X concentration, and $HONO/NO_2$ direct emission ratio, respectively. The direct emission contribution was estimated by comparing the direct emission HONO with the observed HONO. The ranges of $HONO_{emission}$/HONO in CD, PD, and SPD periods were 2–52%, 6–34%, and 2–41%, respectively, and the mean values were 17, 16, and 16%, respectively. The frequency distribution of the $HONO_{emission}$/HONO ratio at nighttime is shown in **Fig. 6**. For this upper limit estimation, the frequency distribution of $HONO_{emission}$/HONO (less than 20%) was approximately 77%. Hence, direct emission may not be the main reason for the high growth of HONO levels. Compared with the direct emission of other sites, that of the measurement site accounted for a lower proportion possibly because the site is relatively far from the highway on the campus.

3.2.3. Heterogeneous conversion of NO_2 to HONO

NO_2 is an important precursor for HONO formation. In addition, recent field measurements in many urban locations have shown that a positive correlation exists between HONO and NO_2 (Cui et al., 2018; Hao et al., 2006; Huang et al., 2017; Zhang et al., 2019), suggesting they have a common source. Moreover, Acker et al. (2005) reported that different meteorological conditions may lead to significant differences in the relationship between the source and receptor, and these differences lead to various types of correlation. During the measurement period, the $HONO/NO_2$ ratio varied between 1.3 and 59.0%, with an average of 7.6%, which is slightly higher than the averaged value of 6.2% in a previous study (Cui et al., 2018). The $HONO/NO_2$ ratio calculated in this work is much larger than that calculated for direct emission (< 1%) (Kurtenbach et al., 2001), suggesting that heterogeneous reactions may be a more important pathway for HONO production than direct emissions. With regard to the heterogeneous conversion of NO_2, several studies (An et al., 2012; Shen and Zhang, 2013) have reported that the surface of soot particles is the medium

of NO_2 conversion. The contribution of soot surface to HONO production is usually much lower than expected because the uptake efficiency of NO_2 decreases with the prolonged reaction time caused by surface deactivation. The aerosol surface is an important medium for the heterogeneous transformation from NO_2 to HONO (Liu et al., 2014). The mass concentration of aerosols was used as an alternative to identify the influence of aerosols in this study because the surface density of aerosols could not be obtained.

The correlations between $PM_{2.5}$ and $HONO/NO_2$ ratio in CD, PD, and SPD periods are shown in **Fig. 7**. With the exacerbation of the $PM_{2.5}$ level, the average value of $HONO/NO_2$ gradually increased, indicating that the aerosol surface occupied an important position in the heterogeneous transformation. A comparison of $HONO/NO_2$ and HONO with $PM_{2.5}$ showed that the correlation between $HONO/NO_2$ and $PM_{2.5}$ (R^2 = 0.23) was weaker than that between HONO and $PM_{2.5}$ (R^2 = 0.55) in the entire period. The main source of HONO could not have been the transformation of NO_2. Notably, the HONO correlation in the PD period was significantly stronger than that in the two other periods. This result proves that HONO-related reactions occurred more frequently during this period. The fair correlation between HONO and $PM_{2.5}$ may pinpoint the mainly anthropogenic origins of these two pollutants with the high direct or indirect contribution of combustion sources. The reason for the increased HONO during the heavy pollution period could be by the comparatively high loading and large particle surface (Cui et al., 2018). Similar phenomena have been observed in a correlation study on CO and HONO wherein CO was used as a tracer for traffic-induced emissions and tested by considering the correlation between HONO and CO over an identical time interval (Qin et al., 2009). The correlation coefficient between HONO and CO was relatively moderate (R^2 = 0.43), indicating that HONO and CO

could come from the same source of emissions. Generally speaking, CO and NO are mainly related to combustion processes such as vehicle emissions, fossil fuel and biomass combustion (Tong et al., 2016). Thus, fossil fuel and biomass combustion may contribute to HONO production, but they can not be measured directly.

The absorbed water influences the heterogeneous formation (Stutz et al., 2004). The influence of RH on the heterogeneous conversion is shown in **Fig. 7(d)**. When RH was less, the HONO/NO_2 ratio slowly increased. When RH was increased, the HONO/NO_2 ratio began to increase rapidly with RH. The HONO/NO_2 ratio decreased when RH reached a certain high level. Similar variation patterns have been obtained in previous studies (Huang et al., 2017; Qin et al., 2009; Tong et al., 2015). Surface adsorbed water functions not only as sources but also as sinks of HONO by affecting the hydrolysis of NO_2 and the sedimentation of HONO to generate HONO (Ammann et al., 1998). When RH ranged at the middle level, the heterogeneous conversion of NO_2 to HONO was more significant than that of deposition. This phenomenon confirms that RH improved the conversion efficiency (Stutz et al., 2004). However, the surface reached saturation when RH reached a certain high level. The excess water restricted NO_2 transformation (Wojtal et al., 2011). The absorption and dissolution of HONO by the saturated surface water layer caused HONO/NO_2 ratio to decrease drastically.

The correlation between $HONO_{correct}$ and NO_2 at nighttime is shown in **Fig. S1**. $HONO_{correct}$ was used in the calculation to exclude the influence of direct emission on NO_2 conversion. The nocturnal variations of $HONO_{correct}$, NO_2, and $HONO_{correct}/NO_2$ ratios in the CD, PD, and SPD periods are presented in **Fig. 8**. The uncertainties of $HONO_{correct}$, NO_2, and $HONO_{correct}/NO_2$ ratios in **Fig. 8** are shown in **Table S4**. In general, the

421 $HONO_{correct}/NO_2$ ratio reached its maximum at or before midnight but
422 decreased after midnight. In the PD and SPD periods, HONO was generated
423 by heterogeneous reaction (R4), and NO_2 decreased after midnight. The
424 production of HONO was equal to its loss (mainly night deposition), and
425 HONO concentration reached a relatively banlance. In the current study,
426 directly emitted HONO state (Stutz, 2002). The weak correlation between
427 nighttime $HONO/NO_2$ and $PM_{2.5}$ can be reasonably explained by the stable
428 $HONO_{correct}/NO_2$ ratio after midnight (Qin et al., 2009). A previous study (Xu
429 et al., 2015) found that a low $HONO_{correct}$ in the first half of the night (19:00–
430 00:00 LT) indicates an important contribution of automobile exhaust
431 emissions, and a low $HONO_{correct}$ in the second half of the night means
432 heterogeneous reactions dominate. Therefore, the heterogeneous reaction
433 conversion rate of HONO was calculated in the current study by using the
434 data of $HONO_{correct}$.

435 The conversion rate of HONO (C_{HONO}) is usually used as an indicator
436 to test the efficiency of NO_2 heterogeneous reactions. Total $HONO_{correct}$ was
437 assumed to be generated by the heterogeneous transformation of NO_2. The
438 formula for the conversion rate of NO_2 (C_{HONO}) is as follows (Su et al.,
439 2008a; Xu et al., 2015):

440 $$C_{HONO} = \frac{([HONO_{correct}]_{t2} - [HONO_{correct}]_{t1}}{(t2 - t1)\,[NO_2]} \quad (3),$$

441 where $[NO_2]$ is the average concentration of NO_2 within the t2–t1 time
442 interval (1 h). In this study, the averaged conversion rate of NO_2 was
443 1.02×10^{-2} h^{-1}. The mean values of C_{HONO} in the CD, PD, and SPD periods
444 were 0.72×10^{-2}, 0.64×10^{-2}, and 1.54×10^{-2} h^{-1}, respectively. The averaged
445 conversion rates in this study were 0.58×10^{-2} and 1.46×10^{-2} h^{-1} higher than
446 those of Beijing I (polluted) and II (heavily polluted) periods, respectively.
447 The increase in the conversion rate demonstrates that NO_2 had high reaction
448 efficiency through the process from NO_2 to HONO in the aggravation of

pollution, which could have led to the high utilization efficiency of the aerosol surface. The exact uptake coefficients of NO_2 on ground and aerosol surfaces are variable and should be different (Harrison and Collins, 1998). The present analysis simplified this process by treating the ground and aerosol surfaces the same. The uptake coefficient is mainly dependent on the surface characteristics, e.g. surface type and moisture (Lu et al., 2018).

3.3. Daytime HONO budget

The expression of d HONO / d t represents the observed variations of hourly HONO concentrations, for which we can use Δ HONO/Δ t instead:

$$\frac{d[HONO]}{dt} = sources - sinks$$

$$= (P_{unknown} + P_{OH+NO} + P_{emi} + P_{het}) - (L_{OH+HONO} + L_{photo}) \quad (4),$$

$$P_{OH+NO} = k_{OH+NO}\,[OH]\,[NO] \quad (5),$$

$$L_{OH+HONO} = k_{OH+HONO}\,[OH]\,[HONO] \quad (6).$$

The d HONO / d t calculated from the measurements was small and evenly distributed around zero (Li et al., 2012). $P_{unknown}$ is the production rate by an unknown daytime HONO source. P_{OH+NO} is the rate of reaction of NO and OH. P_{emi} represents the direct emission rate of HONO from combustion processes. By studying the source and reduction, the daytime HONO budget was analyzed with Eq. (4) (Su et al., 2008b). The heterogeneous transformation mechanism was assumed to be the same for day and night. Therefore, the daytime heterogeneous productivity ($P_{het} = C_{HONO} \times [NO_2]$) was calculated with the nighttime mean values of C_{HONO} in different periods. $L_{OH+HONO}$ is the rate of the reaction between OH and HONO (R3). The calculation formulas of P_{OH+NO} and $L_{OH+HONO}$ have been provided in **Section 3.2.1**. Upon sunlight irradiation, ·OH and NO were formed as R1. L_{photo} represents the photolysis loss rate of HONO ($L_{photo} = J_{HONO} \times [HONO]$). The photolysis frequency and ·OH concentration could not be directly measured in this study. Therefore, the tropospheric ultraviolet and visible (TUV) transfer

model of the National Center for Atmospheric Research (http://cprm.acom.ucar.edu/Models/TUV/ Interactive_TUV/) (Hou et al., 2016) was used to calculate the J_{HONO} value. The J_{HONO} values obtained this way were assumed in clear sky days without clouds. O_3 column and the surface albedo. O_3 column density measured by the Ozone Monitoring Instrument (OMI, data available at https://ozonewatch.gsfc.nasa.gov/data/omi/Y2019/). The O_3 column density ranges from 292 to 306 DU during the entire period. The experimental site being situated in an urban region, the surface albedo is considered as 0.13 (Sailor, 1995). The ground elevation and the measurement altitude are 168 and 188 m respectively. The concentration of OH radicals was calculated with the formulas of NO_2, O_3, and J_{O^1D} in the supplement (Rohrer and Berresheim, 2006). Aerosol effects were considered by using aerosol optical thickness (AOD), single scattering albedo (SSA), and Angstrom exponent as inputs in the TUV model. Typical AOD, SSA, and Angstrom exponent values of 1.32, 0.9, and 1.3, respectively, were adopted for the PD and SPD periods. In the CD period, the respective values were 0.66, 0.89, and 1.07 (Che et al., 2015; Cui et al., 2018; Hou et al., 2016). We wanted to study that under the same output conditions from the TUV model in the PD and SPD periods, the impact of different pollution levels changed on the daytime budget. Hence, the average profiles of J_{HONO} and J_{O^1D} concentrations in the CD, PD, and SPD periods are shown in **Fig. 9**. The mean values of J_{HONO} and ·OH concentration at noon in the CD, PD, and SPD periods were 5.93×10^{-4}, 3.79×10^{-4}, and 3.79×10^{-4} molecule cm^{-3} and 4.10×10^{6}, 2.93×10^{6}, and 3.76×10^{6} molecule cm^{-3}, respectively. The results of the calculated OH radicals ranged from $(0.58-11.49)\times10^{6}$ molecule cm^{-3}, and the mean value was 3.57×10^{6} molecule cm^{-3} at noon in Zhengzhou.

Each production and loss rate of daytime HONO during CD, PD, and SPD periods is illustrated in **Fig. 9** together with dHONO/dt. $P_{unknown}$ was at

a high level before midday. $P_{unknown}$ approached 0 ppbv h^{-1} after midday. In the CD, PD, and SPD periods, the mean values of $P_{unknown}$ were 0.26, 0.40, and 1.83 ppbv h^{-1}, respectively; the mean values of P_{OH+NO} were 1.14, 2.07, and 4.03 ppbv h^{-1}, respectively; the mean values of P_{emi} were 0.17, 0.30, and 0.43 ppbv h^{-1}, respectively; and the mean values of P_{het} were 0.14, 0.18, and 0.55 ppbv h^{-1}, respectively. The midday time $P_{unknown}$ (1.83 ppbv h^{-1}) calculated in Zhengzhou during the winter haze pollution period was close to the result obtained from Beijing's urban area (Hou et al., 2016) (1.85 ppbv h^{-1}). The $P_{unknown}$ contribution to daytime HONO sources in CD, PD, and SPD periods accounted for 15, 14, and 28% of the HONO production rate ($P_{unknown} + P_{OH+NO} + P_{emi} + P_{het}$), respectively. Previous studies (Spataro et al., 2013; Yang et al., 2014) have shown that meteorological conditions, such as solar radiation and WS, can affect unknown sources. The low $P_{unknown}$ contribution of daytime HONO concentration may be related to the low solar radiation and low wind speed during severe pollution. The concentration of NO has a great influence on P_{OH+NO}, so the homogeneous reaction is still an important pathway of HONO production during the daytime. In addition to the photolysis of HONO and the homogeneous reaction of HONO and OH, one or more important sinks might exist to control the variation between the sources and sinks of the daytime HONO during complex contamination. However, further research is needed to analyze the unknown sources of daytime HONO.

4. Conclusions

Ambient HONO measurement using AIM with other atmospheric pollutants and meteorological parameters was conducted in the CPER. The HONO concentrations during the entire measurement varied from 0.2 to 14.8 ppbv, with an average of 2.5 ppbv. The HONO concentrations in the CD, PD, and SPD periods were 1.1, 2.3, and 3.7 ppbv, respectively, and the HONO/NO_2 ratios were 4.7, 7.1, and 9.4%, respectively. HONO concentration was a combined action of direct emission and heterogeneous reaction, and the contributions of the two were higher than that of homogeneous

reaction in the first half of the night. However, the proportion of homogenization gradually increased in the second half of the night due to the steady increase in NO concentration. The hourly level of other HONO abatement pathways aside from OH + HONO should be at least 0.22 ppbv h^{-1} in the SPD period. The sum of the frequency distributions of the $HONO_{emission}$/HONO ratio (less than 20%) was approximately 77%, indicating that the direct emission of HONO was not the main source of the observed HONO level at night. The mean values of $HONO_{emission}$/HONO in the CD, PD, and SPD periods were 17, 16, and 16%, respectively. This phenomenon means that the policy of restricting motor vehicles published by the local government in January 2019 had a good effect on decreasing HONO emissions. In addition, when RH increased at the middle level, the heterogeneous HONO production increased, but it decreased when RH increased further due to the effect of surface water. The contribution of the three sources varied with different pollution levels. The mean values of C_{HONO} in the CD, PD, and SPD periods were 0.72×10^{-2}, 0.64×10^{-2}, and 1.54×10^{-2} h^{-1}, respectively. At nighttime in the SPD period, the heterogeneous conversion of NO_2 appeared to be unimportant. Furthermore, the net production generated by homogeneous reaction may be the leading factor for the increase in HONO under high-NO_X conditions (i.e., the concentration of NO was relatively higher than that of NO_2) at nighttime. The mean value of P_{OH+NO}^{net} in the CD, PD, and SPD periods were 0.13, 0.26, and 0.56 ppbv h^{-1}, respectively. Daytime HONO budget analysis showed that the mean values of $P_{unknown}$ in the CD, PD, and SPD periods were 0.26, 0.40, and 1.83 ppbv h^{-1}, respectively. Although the values of P_{OH+NO} had high uncertainty because of the variation of NO concentrations, P_{OH+NO} contributed the most to HONO production during the daytime. After the analysis, C_{HONO}, P_{OH+NO}^{net}, and $P_{unknown}$ in the SPD period were larger than those in the other periods, indicating that HONO participated in many reactions.

Data availability

All the data used in this paper are available from the corresponding author upon

request (jiangn@zzu.edu.cn).

Author contributions

NJ, RZ, and, SL conceived and designed the study. QH analyzed the data and wrote the paper. LY performed aerosol sampling and data analyses.

Competing interests

The authors declare that they have no conflict of interest.

Acknowledgments

The study was supported by the financial support from the National Natural Science Foundation of China (51808510, 51778587), National Key Research and Development Program of China (2017YFC0212400), Natural Science Foundation of Henan Province of China (162300410255), National Research Program for Key Issues in Air Pollution Control (DQGG0107).

Reference

Acker, K., Möller, D., Auel, R., Wieprecht, W., and Kalaß, D.: Concentrations of nitrous acid, nitric acid, nitrite and nitrate in the gas and aerosol phase at a site in the emission zone during ESCOMPTE 2001 experiment, Atmos. Res., 74, 507-524, https://doi.org/10.1016/j.atmosres.2004.04.009, 2005.

Alicke, B., Platt, U., and Stutz, J.: Impact of nitrous acid photolysis on the total hydroxyl radical budget during the Limitation of Oxidant Production/Pianura Padana Produzione di Ozono study in Milan, J. Geophys. Res., https://doi.org/10.1029/2000jd000075, 2002.

Alicke, B., Geyer, A., Hofzumahaus, A., and Holland, F.: OH formation by HONO photolysis during the BERLIOZ experiment, J. Geophys. Res., 108, https://doi.org/10.1029/2001jd000579, 2003.

Ammann, M., Kalberer, M., Jost, D. T., Tobler, L., Rössler, E., Piguet, D., Gäggeler, H. W., and Baltensperger, U.: Heterogeneous production of nitrous acid on soot in polluted air masses, Nature, 395, 157-160, https://doi.org/10.1038/25965, 1998.

An, J., Li, Y., Chen, Y., Li, J., Qu, Y., and Tang, Y.: Enhancements of major aerosol components due to additional HONO sources in the North China Plain and implications for visibility and haze, Adv. Atoms. Sci., 30, 57-66, https://doi.org/10.1007/s00376-012-2016-9, 2012.

Atkinson, R., Baulch, D. L., Cox, R. A., Crowley, J. N., Hampson, R. F., Hynes, R. G., Jenkin, M. E., Rossi, M. J., and Troe, J.: Evaluated kinetic and photochemical data for atmospheric chemistry: Volume I - gas phase reactions of O_x, HO_x, NO_x and SO_x species, Atmos. Chem. Phys., 4, 1461-1738, https://doi.org/10.5194/acp-4-1461-2004, 2004.

Che, H., Xia, X., Zhu, J., Wang, H., Wang, Y., Sun, J., Zhang, X., and Shi, G.: Aerosol optical properties under the condition of heavy haze over an urban site of Beijing, China, Environ. Sci. Pollut. Res., 22, 1043-1053, https://doi.org/10.1007/s11356-014-3415-5, 2015.

Cui, L., Li, R., Zhang, Y., Meng, Y., Fu, H., and Chen, J.: An observational study of nitrous acid (HONO) in Shanghai, China: The aerosol impact on HONO formation during the haze episodes, Sci. Total Environ., 630, 1057-1070, https://doi.org/10.1016/j.scitotenv.2018.02.063, 2018.

Czader, B. H., Rappenglück, B., Percell, P., Byun, D. W., Ngan, F., and Kim, S.: Modeling nitrous acid and its impact on ozone and hydroxyl radical during the Texas Air Quality Study 2006, Atmos. Chem. Phys., 12, 6939-6951, https://doi.org/10.5194/acp-12-6939-2012, 2012.

Dong, Z., Jiang, N., Duan, S., Zhang, L., Li, S., and Zhang, R.: Size distributions and size-segregated chemical profiles of particulate matter in a traffic tunnel of East-Central China, Atmos. Pollut. Res., 10, 1873-1883, https://doi.org/10.1016/j.apr.2019.08.001, 2019.

Duan, J., Qin, M., Ouyang, B., Fang, W., Li, X., Lu, K., Tang, K., Liang, S., Meng, F., Hu, Z., Xie, P., Liu, W., and Häsler, R.: Development of an incoherent broadband cavity-enhanced absorption spectrometer for in situ measurements of HONO and NO_2, Atmos. Meas. Tech., 11, 4531-4543, https://doi.org/10.5194/amt-11-4531-2018, 2018.

Elshorbany, Y. F., Steil, B., Brühl, C., and Lelieveld, J.: Impact of HONO on global atmospheric chemistry calculated with an empirical parameterization in the EMAC model, Atmos. Chem. Phys., 12, 9977-10000, https://doi.org/10.5194/acp-12-9977-2012, 2012.

Elshorbany, Y. F., Crutzen, P. J., Steil, B., Pozzer, A., Tost, H., and Lelieveld, J.: Global and regional impacts of HONO on the chemical composition of clouds and aerosols, Atmos. Chem. Phys., 14, 1167-1184, https://doi.org/10.5194/acp-14-1167-2014, 2014.

Finlayson-Pitts, B. J., Wingen, L. M., Sumner, A. L., Syomin, D., and Ramazan, K. A.: The heterogeneous hydrolysis of NO2 in laboratory systems and in outdoor and

indoor atmospheres: An integrated mechanism, PCCP, 5, 223-242, https://doi.org/10.1039/b208564j, 2003.

Grassian, V. H.: Heterogeneous uptake and reaction of nitrogen oxides and volatile organic compounds on the surface of atmospheric particles including oxides, carbonates, soot and mineral dust: Implications for the chemical balance of the troposphere, Int. Rev. Phys. Chem., 20, 467-548, https://doi.org/10.1080/01442350110051968, 2001.

Hao, N., Zhou, B., Chen, D., and Chen, L.: Observations of nitrous acid and its relative humidity dependence in Shanghai, J. Environ. Sci.-China, 18, 910-915, https://doi.org/10.1016/s1001-0742(06)60013-2, 2006.

Harrison, R. M., Peak, J. D., and Collins, G. M.: Tropospheric cycle of nitrous acid, J. Geophys. Res., 101, 14429-14439, https://doi.org/10.1029/96jd00341, 1996.

Harrison, R. M., and Collins, G. M.: Measurements of Reaction Coefficients of NO2 and HONO on Aerosol Particles, J. Atmos. Chem., 30, 397-406, https://doi.org/10.1023/A:1006094304069, 1998.

Heland, J., Kleffmann, J., Kurtenbach, R., and Wiesen, P.: A new instrument to measure gaseous nitrous acid (HONO) in the atmosphere, Environ. Sci. Technol., 35, 3207-3212, https://doi.org/10.1021/es000303t, 2001.

Hendrick, F., Müller, J. F., Clémer, K., Wang, P., De Mazière, M., Fayt, C., Gielen, C., Hermans, C., Ma, J. Z., Pinardi, G., Stavrakou, T., Vlemmix, T., and Van Roozendael, M.: Four years of ground-based MAX-DOAS observations of HONO and NO_2 in the Beijing area, Atmos. Chem. Phys., 14, 765-781, https://doi.org/10.5194/acp-14-765-2014, 2014.

Hirokawa, J., Kato, T., and Mafuné, F.: In Situ Measurements of Atmospheric Nitrous Acid by Chemical Ionization Mass Spectrometry Using Chloride Ion Transfer Reactions, Anal. Chem., 81, 8380-8386, https://doi.org/10.1021/ac901117b, 2009.

654 Hou, S., Tong, S., Ge, M., and An, J.: Comparison of atmospheric nitrous acid during
655 severe haze and clean periods in Beijing, China, Atmos. Environ., 124, 199-206,
656 https://doi.org/10.1016/j.atmosenv.2015.06.023, 2016.
657 Huang, R.-J., Yang, L., Cao, J., Wang, Q., Tie, X., Ho, K.-F., Shen, Z., Zhang, R., Li,
658 G., Zhu, C., Zhang, N., Dai, W., Zhou, J., Liu, S., Chen, Y., Chen, J., and O'Dowd,
659 C. D.: Concentration and sources of atmospheric nitrous acid (HONO) at an urban
660 site in Western China, Sci. Total Environ., 593-594, 165-172,
661 https://doi.org/10.1016/j.scitotenv.2017.02.166, 2017.
662 Jiang, N., Guo, Y., Wang, Q., Kang, P., Zhang, R., and Tang, X.: Chemical
663 composition characteristics of $PM_{2.5}$ in three cities in Henan, Central China,
664 Aerosol Air Qual. Res., 17, 2367-2380, https://doi.org/10.4209/aaqr.2016.10.0463,
665 2017.
666 Jiang, N., Dong, Z., Xu, Y., Yu, F., Yin, S., Zhang, R., and Tang, X.: Characterization
667 of PM_{10} and $PM_{2.5}$ Source Profiles of Fugitive Dust in Zhengzhou, China, Aerosol
668 Air Qual. Res., 18, 314-329, https://doi.org/10.4209/aaqr.2017.04.0132, 2018a.
669 Jiang, N., Duan, S., Yu, X., Zhang, R., and Wang, K.: Comparative major components
670 and health risks of toxic elements and polycyclic aromatic hydrocarbons of $PM_{2.5}$
671 in winter and summer in Zhengzhou: Based on three-year data, Atmos. Res., 213,
672 173-184, https://doi.org/10.1016/j.atmosres.2018.06.008, 2018b.
673 Jiang, N., Li, Q., Su, F., Wang, Q., Yu, X., Kang, P., Zhang, R., and Tang, X.:
674 Chemical characteristics and source apportionment of $PM_{2.5}$ between heavily
675 polluted days and other days in Zhengzhou, China, J. Environ. Sci.-China, 66, 188-
676 198, https://doi.org/10.1016/j.jes.2017.05.006, 2018c.
677 Jiang, N., Wang, K., Yu, X., Su, F., Yin, S., Li, Q., and Zhang, R.: Chemical
678 characteristics and source apportionment by two receptor models of size-segregated
679 aerosols in an emerging megacity in China, Aerosol Air Qual. Res., 18, 1375–1390,
680 https://doi.org/10.4209/aaqr.2017.10.0413, 2018d.

Jiang, N., Yin, S., Guo, Y., Li, J., Kang, P., Zhang, R., and Tang, X.: Characteristics of mass concentration, chemical composition, source apportionment of $PM_{2.5}$ and PM_{10} and health risk assessment in the emerging megacity in China, Atmos. Pollut. Res., 9, 2367–2380, https://doi.org/10.1016/j.apr.2017.07.005, 2018e.

Jiang, N., Li, L., Wang, S., Li, Q., Dong, Z., Duan, S., Zhang, R., and Li, S.: Variation tendency of pollution characterization, sources, and health risks of $PM_{2.5}$-bound polycyclic aromatic hydrocarbons in an emerging megacity in China: Based on three-year data, Atmos. Res., 217, 81-92, https://doi.org/10.1016/j.atmosres.2018.10.023, 2019a.

Jiang, N., Liu, X., Wang, S., Yu, X., Yin, S., Duan, S., Shenbo, W., Zhang, R., and Li, S.: Pollution characterization, source identification, and health risks of atmospheric-particle-bound heavy metals in PM_{10} and $PM_{2.5}$ at multiple sites in an emerging megacity in the Central Region of China, Aerosol Air Qual. Res., 19, 247-271, https://doi.org/10.4209/aaqr.2018.07.0275, 2019b.

Kim, D.-R., Lee, J.-B., Keun Song, C., Kim, S.-Y., Ma, Y.-l., Lee, K.-M., Cha, J.-S., and Lee, S.-D.: Temporal and spatial distribution of tropospheric NO_2 over Northeast Asia using OMI data during the years 2005–2010, Atmos. Pollut. Res., 6, 768-776, https://doi.org/10.5094/apr.2015.085, 2015.

Kleffmann, J., Becker, K. H., Lackhoff, M., and Wiesen, P.: Heterogeneous conversion of NO2 on carbonaceous surfaces, PCCP, 1, 5443-5450, https://doi.org/10.1039/a905545b, 1999.

Kurtenbach, R., Becker, K. H., Gomes, J. A. G., Kleffmann, J., Lorzer, J. C., Spittler, M., Wiesen, P., Ackermann, R., Geyer, A., and Platt, U.: Investigations of emissions and heterogeneous formation of HONO in a road traffic tunnel, Atmos. Environ., 35, 3385-3394, https://doi.org/10.1016/s1352-2310(01)00138-8, 2001.

Lelieveld, J., Gromov, S., Pozzer, A., and Taraborrelli, D.: Global tropospheric hydroxyl distribution, budget and reactivity, Atmos. Chem. Phys., 16, 12477-12493, https://doi.org/10.5194/acp-16-12477-2016, 2016.

Li, Q., Jiang, N., Yu, X., Dong, Z., Duan, S., Zhang, L., and Zhang, R.: Sources and spatial distribution of $PM_{2.5}$-bound polycyclic aromatic hydrocarbons in Zhengzhou in 2016, Atmos. Res., 216, 65–75, https://doi.org/10.1016/j.atmosres.2018.09.011, 2019.

Li, X., Brauers, T., Häseler, R., Bohn, B., Fuchs, H., Hofzumahaus, A., Holland, F., Lou, S., Lu, K. D., Rohrer, F., Hu, M., Zeng, L. M., Zhang, Y. H., Garland, R. M., Su, H., Nowak, A., Wiedensohler, A., Takegawa, N., Shao, M., and Wahner, A.: Exploring the atmospheric chemistry of nitrous acid (HONO) at a rural site in Southern China, Atmos. Chem. Phys., 12, 1497-1513, https://doi.org/10.5194/acp-12-1497-2012, 2012.

Liu, F., Beirle, S., Zhang, Q., van der A, R. J., Zheng, B., Tong, D., and He, K.: NOx emission trends over Chinese cities estimated from OMI observations during 2005 to 2015, Atmos Chem Phys, 17, 9261-9275, https://doi.org/10.5194/acp-17-9261-2017, 2017.

Liu, X., Jiang, N., Yu, X., Zhang, R., Li, S., Li, Q., and Kang, P.: Chemical characteristics, sources apportionment, and risk assessment of $PM_{2.5}$ in different functional areas of an emerging megacity in China, Aerosol Air Qual. Res., 19, 2222-2238, https://doi.org/10.4209/aaqr.2019.02.0076, 2019.

Liu, Z., Wang, Y., Costabile, F., Amoroso, A., Zhao, C., Huey, L. G., Stickel, R., Liao, J., and Zhu, T.: Evidence of aerosols as a media for rapid daytime HONO production over China, Environ. Sci. Technol., 48, 14386-14391, https://doi.org/10.1021/es504163z, 2014.

Lu, X., Wang, Y., Li, J., Shen, L., and Fung, J. C. H.: Evidence of heterogeneous HONO formation from aerosols and the regional photochemical impact of this HONO source, Environ. Res. Lett., 13, https://doi.org/10.1088/1748-9326/aae492, 2018.

Markovic, M. Z., VandenBoer, T. C., and Murphy, J. G.: Characterization and optimization of an online system for the simultaneous measurement of atmospheric

water-soluble constituents in the gas and particle phases, J. Environ. Monit., 14, 1872-1884, https://doi.org/10.1039/c2em00004k, 2012.

Michoud, V., Colomb, A., Borbon, A., Miet, K., Beekmann, M., Camredon, M., Aumont, B., Perrier, S., Zapf, P., Siour, G., Ait-Helal, W., Afif, C., Kukui, A., Furger, M., Dupont, J. C., Haeffelin, M., and Doussin, J. F.: Study of the unknown HONO daytime source at a European suburban site during the MEGAPOLI summer and winter field campaigns, Atmos. Chem. Phys., 14, 2805-2822, https://doi.org/10.5194/acp-14-2805-2014, 2014.

Min, K. E., Washenfelder, R. A., Dubé, W. P., Langford, A. O., Edwards, P. M., Zarzana, K. J., Stutz, J., Lu, K., Rohrer, F., Zhang, Y., and Brown, S. S.: A broadband cavity enhanced absorption spectrometer for aircraft measurements of glyoxal, methylglyoxal, nitrous acid, nitrogen dioxide, and water vapor, Atmos. Meas. Tech., 9, 423-440, https://doi.org/10.5194/amt-9-423-2016, 2016.

Pinto, J. P., Dibb, J., Lee, B. H., Rappenglück, B., Wood, E. C., Levy, M., Zhang, R. Y., Lefer, B., Ren, X. R., Stutz, J., Tsai, C., Ackermann, L., Golovko, J., Herndon, S. C., Oakes, M., Meng, Q. Y., Munger, J. W., Zahniser, M., and Zheng, J.: Intercomparison of field measurements of nitrous acid (HONO) during the SHARP campaign, J. Geophys. Res.-Atmos., 119, 5583-5601, https://doi.org/10.1002/2013jd020287, 2014.

Qin, M., Xie, P., Su, H., Gu, J., Peng, F., Li, S., Zeng, L., Liu, J., Liu, W., and Zhang, Y.: An observational study of the HONO–NO_2 coupling at an urban site in Guangzhou City, South China, Atmos. Environ., 43, 5731-5742, https://doi.org/10.1016/j.atmosenv.2009.08.017, 2009.

Rappenglück, B., Lubertino, G., Alvarez, S., Golovko, J., Czader, B., and Ackermann, L.: Radical precursors and related species from traffic as observed and modeled at an urban highway junction, J. Air Waste Manage. Assoc., 63, 1270-1286, https://doi.org/10.1080/10962247.2013.822438, 2013.

764 Roberts, J. M., Veres, P., Warneke, C., Neuman, J. A., Washenfelder, R. A., Brown, S.
765 S., Baasandorj, M., Burkholder, J. B., Burling, I. R., Johnson, T. J., Yokelson, R. J.,
766 and de Gouw, J.: Measurement of HONO, HNCO, and other inorganic acids by
767 negative-ion proton-transfer chemical-ionization mass spectrometry (NI-PT-
768 CIMS): application to biomass burning emissions, Atmos. Meas. Tech., 3, 981-990,
769 https://doi.org/10.5194/amt-3-981-2010, 2010.
770 Rohrer, F., and Berresheim, H.: Strong correlation between levels of tropospheric
771 hydroxyl radicals and solar ultraviolet radiation, Nature, 442, 184-187,
772 https://doi.org/10.1038/nature04924, 2006.
773 Sailor, D. J.: Simulated Urban Climate Response to Modifications in Surface Albedo
774 and Vegetative Cover, J. Appl. Meteorol., 34, 1694-1704,
775 https://doi.org/10.1175/1520-0450-34.7.1694, 1995.
776 Sander, S., Friedl, R., Golden, D., Kurylo, M., Huie, R., Orkin, V., Moortgat, G.,
777 Ravishankara, A. R., Kolb, C., Molina, M., and Finlayson-Pitts, B.: Chemical
778 Kinetics and Photochemical Data for Use in Atmospheric Studies; JPL Publication
779 02-25, 2003.
780 Shen, L. J., and Zhang, Z. F.: Heterogeneous reactions of NO_2 on the surface of black
781 carbon, Prog. Chem., 25, 28-35, 2013.
782 Sörgel, M., Regelin, E., Bozem, H., Diesch, J. M., Drewnick, F., Fischer, H., Harder,
783 H., Held, A., Hosaynali-Beygi, Z., Martinez, M., and Zetzsch, C.: Quantification of
784 the unknown HONO daytime source and its relation to NO_2, Atmos. Chem. Phys.,
785 11, 10433-10447, https://doi.org/10.5194/acp-11-10433-2011, 2011.
786 Spataro, F., Ianniello, A., Esposito, G., Allegrini, I., Zhu, T., and Hu, M.: Occurrence
787 of atmospheric nitrous acid in the urban area of Beijing (China), Sci. Total
788 Environ., 447, 210-224, https://doi.org/10.1016/j.scitotenv.2012.12.065, 2013.
789 Stutz, J.: Nitrous acid formation in the urban atmosphere: Gradient measurements of
790 NO_2 and HONO over grass in Milan, Italy, J. Geophys. Res., 107,
791 https://doi.org/10.1029/2001jd000390, 2002.

Stutz, J., Alicke, B., Ackermann, R., Geyer, A., Wang, S., White, A. B., Williams, E. J., Spicer, C. W., and Fast, J. D.: Relative humidity dependence of HONO chemistry in urban areas, J. Geophys. Res., 109, 03307-03319, https://doi.org/10.1029/2003jd004135, 2004.

Su, H., Cheng, Y. F., Cheng, P., Zhang, Y. H., Dong, S., Zeng, L. M., Wang, X., Slanina, J., Shao, M., and Wiedensohler, A.: Observation of nighttime nitrous acid (HONO) formation at a non-urban site during PRIDE-PRD2004 in China, Atmos. Environ., 42, 6219-6232, https://doi.org/10.1016/j.atmosenv.2008.04.006, 2008a.

Su, H., Cheng, Y. F., Shao, M., Gao, D. F., Yu, Z. Y., Zeng, L. M., Slanina, J., Zhang, Y. H., and Wiedensohler, A.: Nitrous acid (HONO) and its daytime sources at a rural site during the 2004 PRIDE-PRD experiment in China, J. Geophys. Res., 113, D14312-14321, https://doi.org/10.1029/2007jd009060, 2008b.

Tan, Z., Rohrer, F., Lu, K., Ma, X., Bohn, B., Broch, S., Dong, H., Fuchs, H., Gkatzelis, G. I., Hofzumahaus, A., Holland, F., Li, X., Liu, Y., Liu, Y., Novelli, A., Shao, M., Wang, H., Wu, Y., Zeng, L., Hu, M., Kiendler-Scharr, A., Wahner, A., and Zhang, Y.: Wintertime photochemistry in Beijing: observations of RO_x radical concentrations in the North China Plain during the BEST-ONE campaign, Atmos. Chem. Phys., 18, 12391-12411, https://doi.org/10.5194/acp-18-12391-2018, 2018.

Tong, S., Hou, S., Zhang, Y., Chu, B., Liu, Y., He, H., Zhao, P., and Ge, M.: Comparisons of measured nitrous acid (HONO) concentrations in a pollution period at urban and suburban Beijing, in autumn of 2014, Sci. China Chem., 58, 1393-1402, https://doi.org/10.1007/s11426-015-5454-2, 2015.

Tong, S., Hou, S., Zhang, Y., Chu, B., Liu, Y., He, H., Zhao, P., and Ge, M.: Exploring the nitrous acid (HONO) formation mechanism in winter Beijing: direct emissions and heterogeneous production in urban and suburban areas, Faraday Discuss., 189, 213-230, https://doi.org/10.1039/c5fd00163c, 2016.

VandenBoer, T. C., Markovic, M. Z., Sanders, J. E., Ren, X., Pusede, S. E., Browne, E. C., Cohen, R. C., Zhang, L., Thomas, J., Brune, W. H., and Murphy, J. G.:

820 Evidence for a nitrous acid (HONO) reservoir at the ground surface in Bakersfield,
821 CA, during CalNex 2010, J. Geophys. Res.-Atmos., 119, 9093-9106,
822 https://doi.org/10.1002/2013jd020971, 2014.
823 Vogel, B., Vogel, H., Kleffmann, J., and Kurtenbach, R.: Measured and simulated
824 vertical profiles of nitrous acid—Part II. Model simulations and indications for a
825 photolytic source, Atmos. Environ., 37, 2957-2966, https://doi.org/10.1016/s1352-
826 2310(03)00243-7, 2003.
827 Wang, S., Zhou, R., Zhao, H., Wang, Z., Chen, L., and Zhou, B.: Long-term
828 observation of atmospheric nitrous acid (HONO) and its implication to local NO_2
829 levels in Shanghai, China, Atmos. Environ., 77, 718-724,
830 https://doi.org/10.1016/j.atmosenv.2013.05.071, 2013.
831 Wang, S., Yin, S., Zhang, R., Yang, L., Zhao, Q., Zhang, L., Yan, Q., Jiang, N., and
832 Tang, X.: Insight into the formation of secondary inorganic aerosol based on high-
833 time-resolution data during haze episodes and snowfall periods in Zhengzhou,
834 China, Sci. Total Environ., 660, 47-56,
835 https://doi.org/10.1016/j.scitotenv.2018.12.465, 2019.
836 Winer, A. M., and Biermann, H. W.: Long pathlength differential optical absorption
837 spectroscopy (DOAS) measurements of gaseous HONO, NO_2 and HCNO in the
838 California South Coast Air Basin, Res. Chem. Intermed., 20, 423-445,
839 https://doi.org/10.1163/156856794X00405, 1994.
840 Wojtal, P., Halla, J. D., and McLaren, R.: Pseudo steady states of HONO measured in
841 the nocturnal marine boundary layer: a conceptual model for HONO formation on
842 aqueous surfaces, Atmos. Chem. Phys., 11, 3243-3261, https://doi.org/10.5194/acp-
843 11-3243-2011, 2011.
844 Xu, Z., Wang, T., Wu, J., Xue, L., Chan, J., Zha, Q., Zhou, S., Louie, P. K. K., and
845 Luk, C. W. Y.: Nitrous acid (HONO) in a polluted subtropical atmosphere:
846 Seasonal variability, direct vehicle emissions and heterogeneous production at

ground surface, Atmos. Environ., 106, 100-109, https://doi.org/10.1016/j.atmosenv.2015.01.061, 2015.

Yang, L., Wang, S., Duan, S., Yan, Q., Jiang, N., Zhang, R., and Li, S.: Characteristics and formation mechanisms of secondary inorganic ions in $PM_{2.5}$ during winter in a central city of China: Based on a high time resolution data, Atmos. Res., 233, https://doi.org/10.1016/j.atmosres.2019.104696, 2020.

Yang, Q., Su, H., Li, X., Cheng, Y., Lu, K., Cheng, P., Gu, J., Guo, S., Hu, M., Zeng, L., Zhu, T., and Zhang, Y.: Daytime HONO formation in the suburban area of the megacity Beijing, China, Sci. China Chem., 57, 1032-1042, https://doi.org/10.1007/s11426-013-5044-0, 2014.

Zhang, B., and Tao, F.-M.: Direct homogeneous nucleation of NO2, H2O, and NH3 for the production of ammonium nitrate particles and HONO gas, Chem. Phys. Lett., 489, 143-147, https://doi.org/10.1016/j.cplett.2010.02.059, 2010.

Zhang, W., Tong, S., Ge, M., An, J., Shi, Z., Hou, S., Xia, K., Qu, Y., Zhang, H., Chu, B., Sun, Y., and He, H.: Variations and sources of nitrous acid (HONO) during a severe pollution episode in Beijing in winter 2016, Sci. Total Environ., 648, 253-262, https://doi.org/10.1016/j.scitotenv.2018.08.133, 2019.

Figure Captions:

Fig. 1. Temporal trends of hourly average T, RH, WD, WS, and $PM_{2.5}$ during the measurement. (The shaded areas: white for the CD period; gray for the PD period; red for the SPD period.)

Fig. 2. Temporal variations of hourly average HONO, NO, NO_2, O_3, and CO during the measurement. (The shaded areas: white for the CD period; gray for the PD period; red for the SPD period.)

Fig. 3. Diurnal variations of HONO during the measurement.

Fig. 4. Diurnal variations of HONO, NO, NO_2, O_3, HONO/NO_2, and HONO/NO_X. The blue points and lines represented the CD period; the black points and lines represented the PD period; the red points and lines represented the SPD period.

Fig. 5. Nocturnal variations of $\mathbf{P_{OH+NO}^{net}}$, HONO and NO during CD, PD and SPD periods.

Fig. 6. Percentage distribution of the nighttime $HONO_{emission}$/HONO. (The dotted line represents the average of $HONO_{emission}$/HONO.)

Fig. 7. Nighttime correlation studies between $PM_{2.5}$ and HONO/NO_2, $PM_{2.5}$ and HONO, CO and HONO, RH and HONO/NO_2 during the entire measurement period, CD, PD, and SPD periods. The blue represented the full measurement period; the light blue represented CD period; the black represented PD period; the red represented SPD period.

Fig. 8. Nocturnal variations of $HONO_{correct}$, NO_2, and $HONO_{correct}/NO_2$ in CD, PD and SPD periods.

Fig. 9. The average profiles of J_{HONO} and J_{O^1D} concentrations during the daytime, and production and loss rate of the daytime HONO in CD, PD and SPD periods.

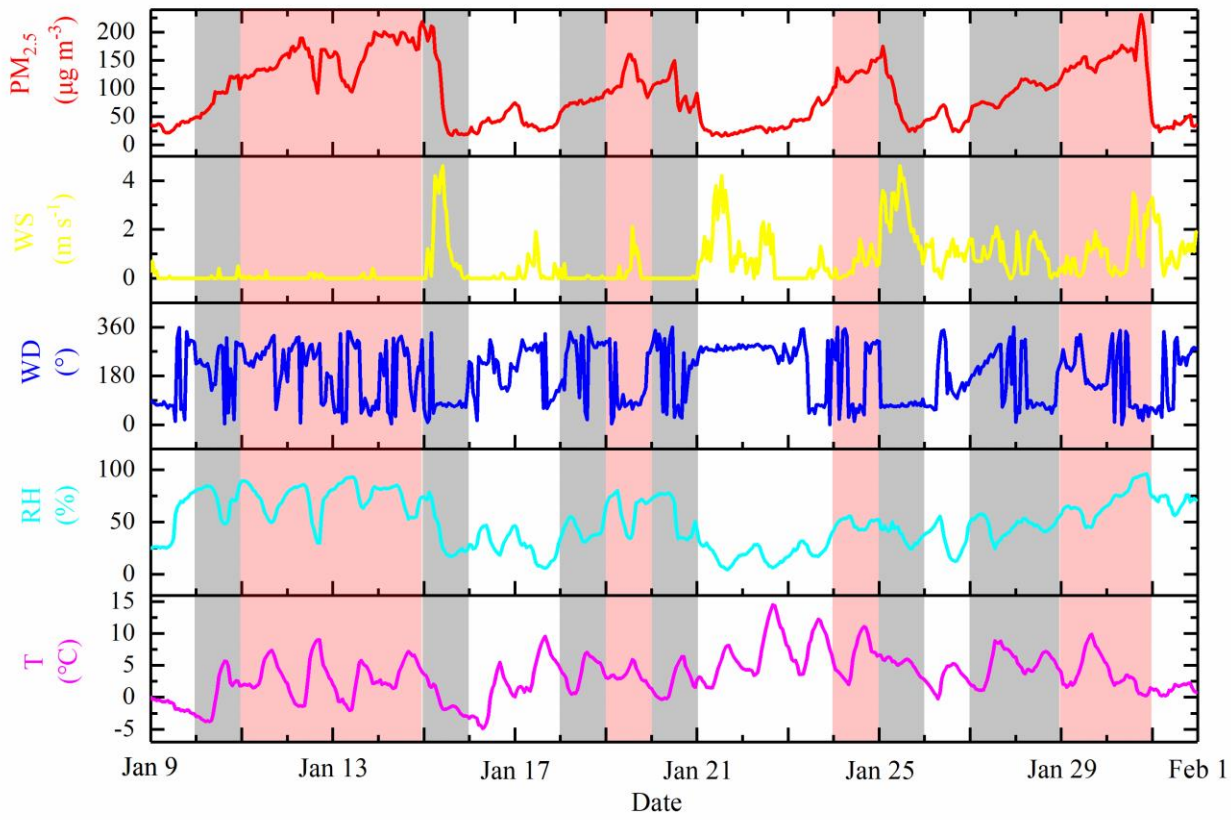

Fig. 1. Temporal trends of hourly average T, RH, WD, WS, and $PM_{2.5}$ during the measurement. (The shaded areas: white for the CD period; gray for the PD period; red for the SPD period.)

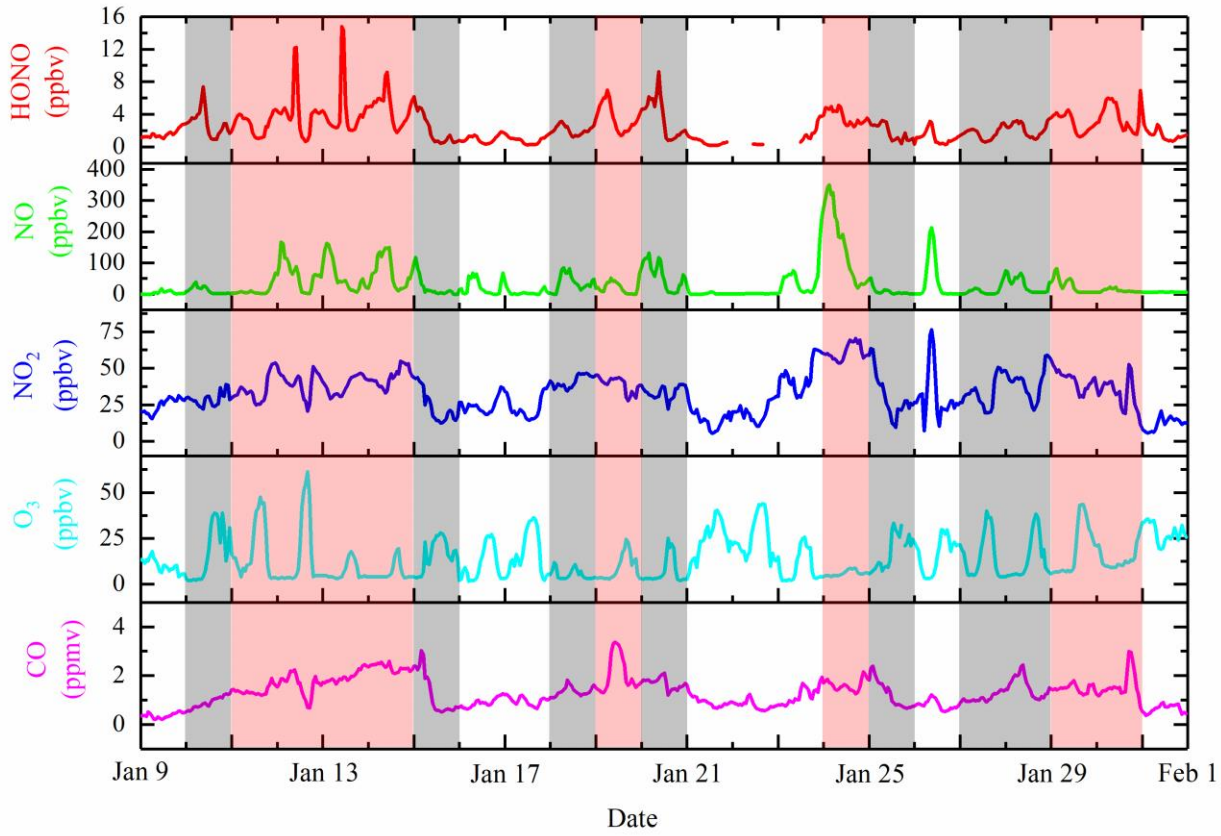

Fig. 2. Temporal variations of hourly average HONO, NO, NO_2, O_3, and CO during the measurement. (The shaded areas: white for the CD period; gray for the PD period; red for the SPD period.)

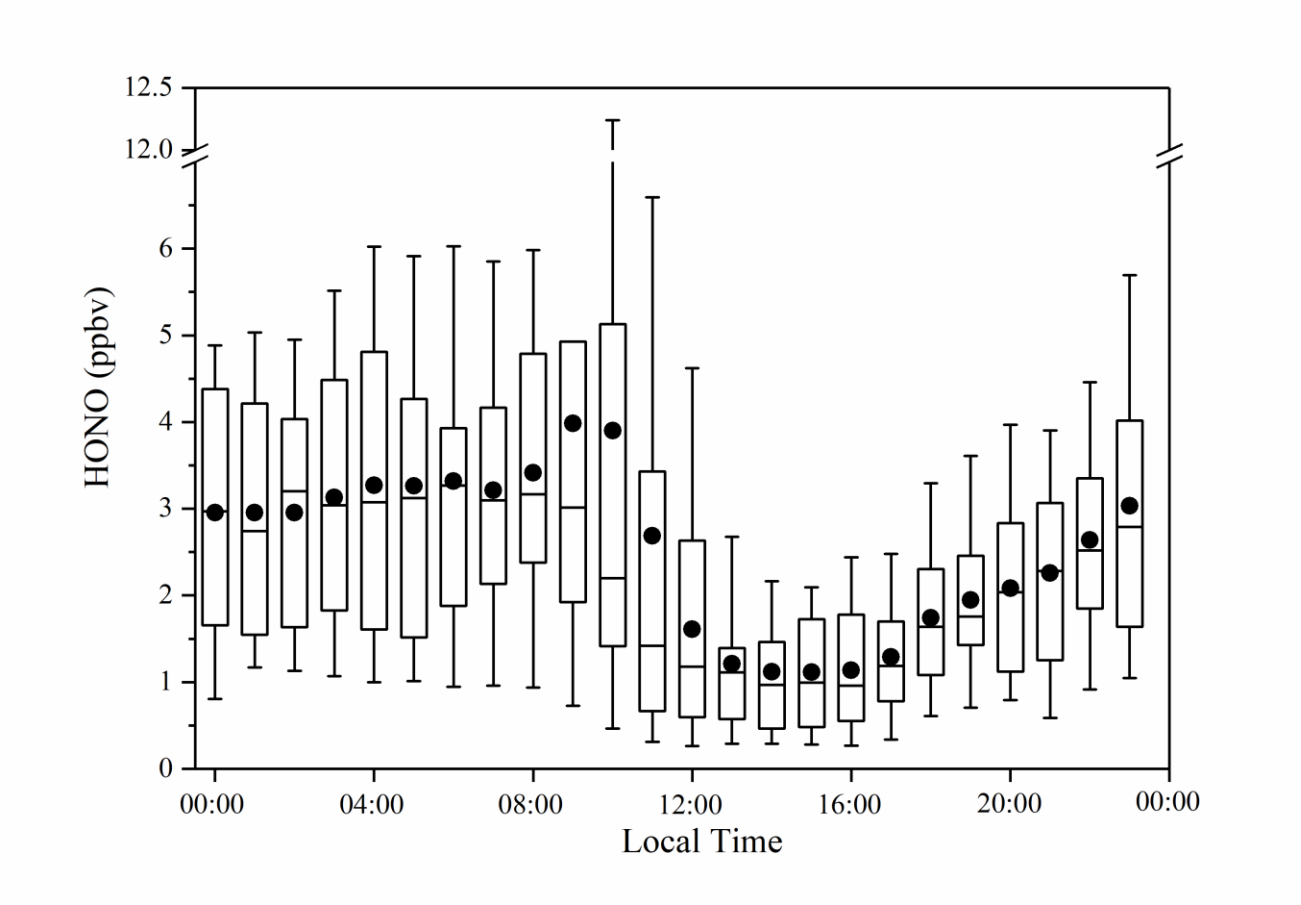

Fig. 3. Diurnal variations of HONO during the measurement.

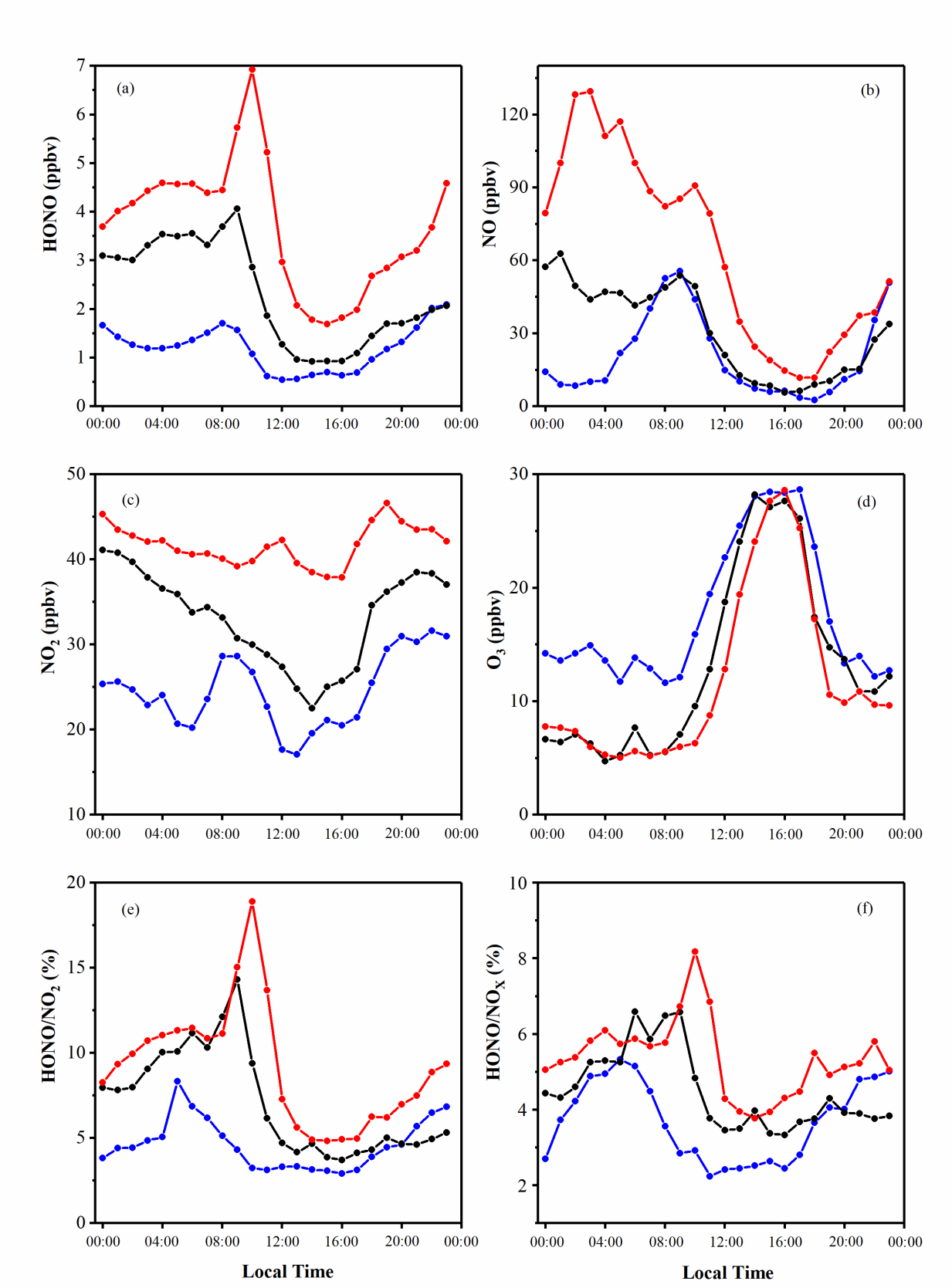

Fig. 4. Diurnal variations of HONO, NO, NO_2, O_3, $HONO/NO_2$, and $HONO/NO_X$. The blue points and lines represented the CD period; the black points and lines represented the PD period; the red points and lines represented the SPD period.

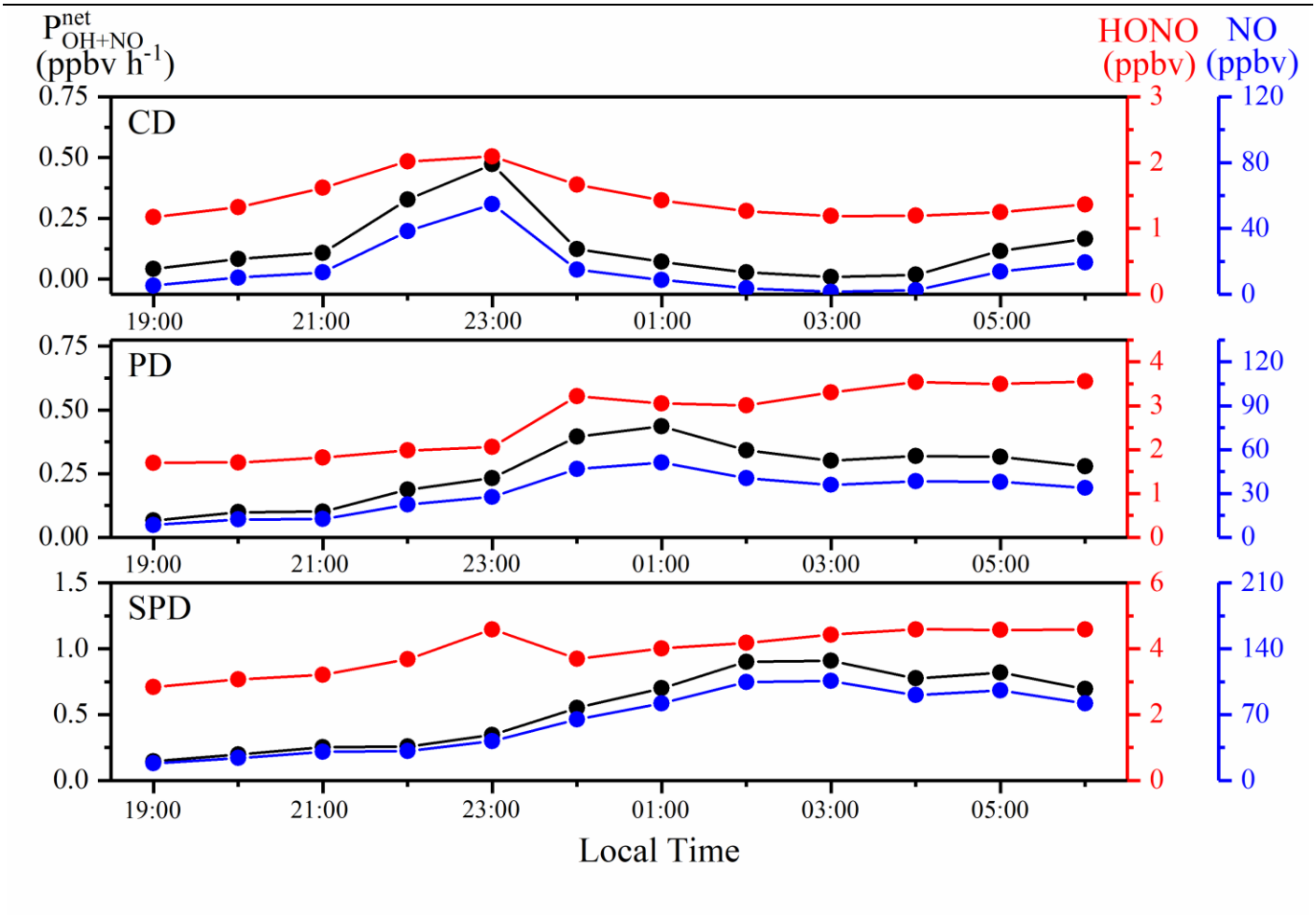

Fig. 5. Nocturnal variations of P^{net}_{OH+NO}, HONO and NO during CD, PD and SPD periods.

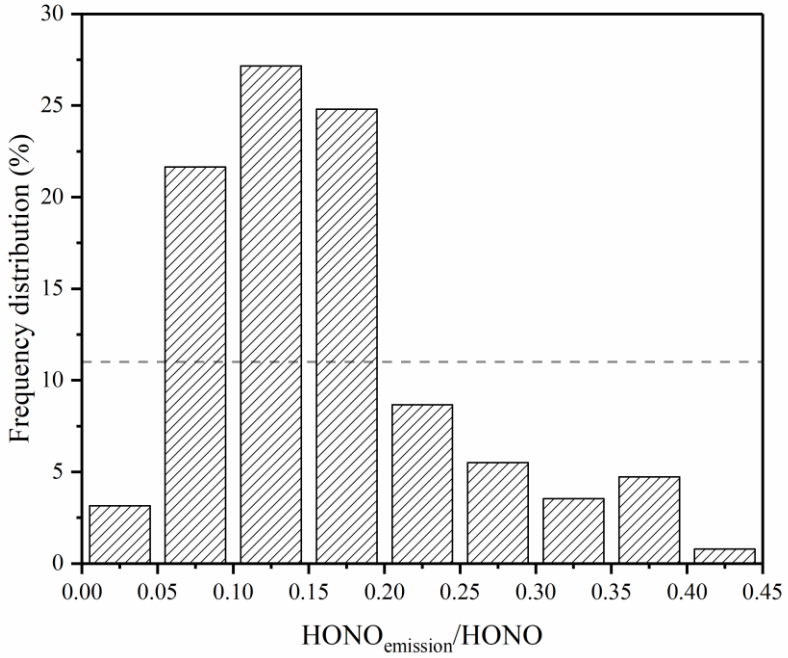

Fig. 6. Percentage distribution of the nighttime $HONO_{emission}/HONO$. (The dotted line represents the average of $HONO_{emission}/HONO$.)

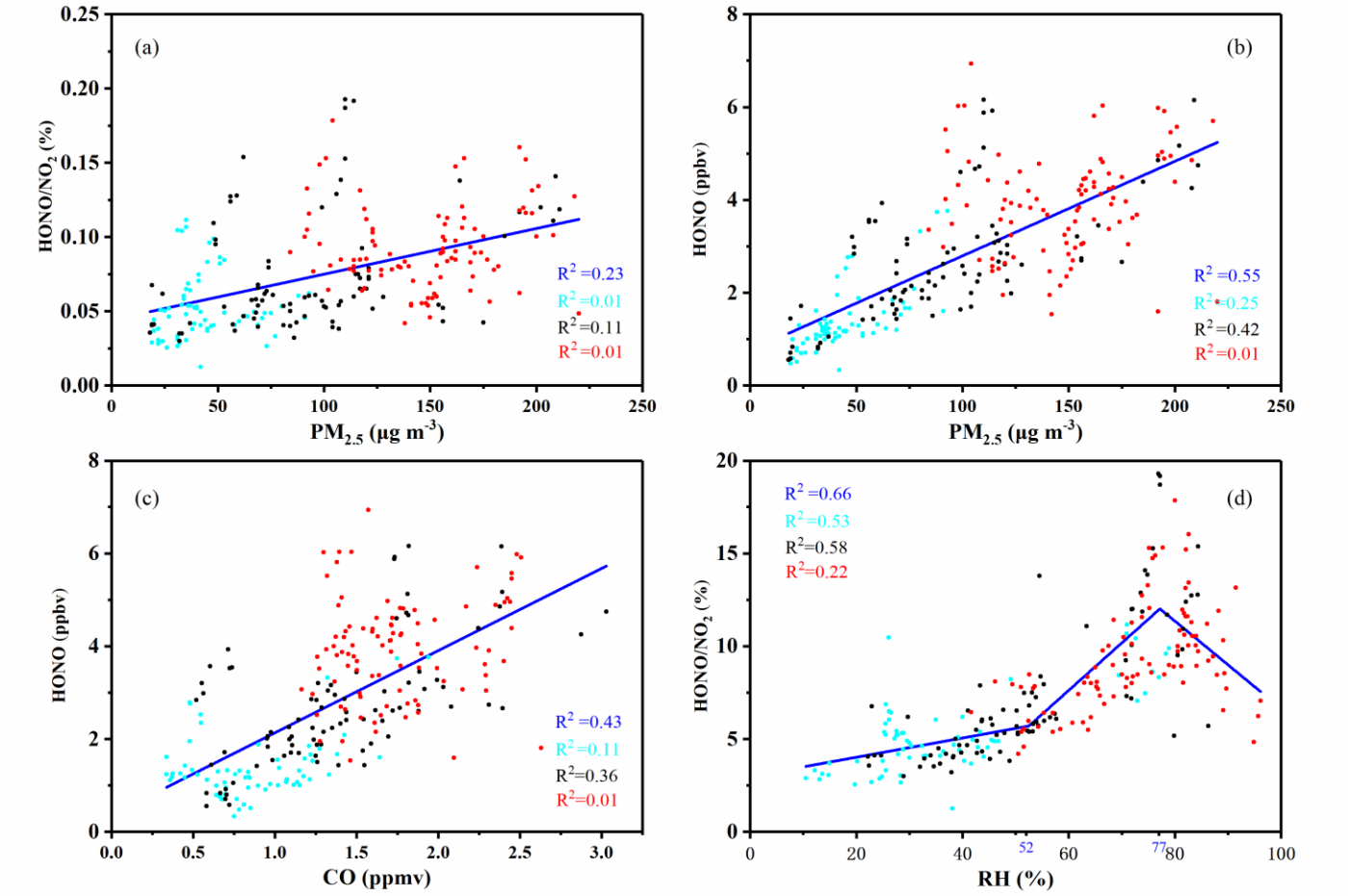

Fig. 7. Nighttime correlation studies between $PM_{2.5}$ and $HONO/NO_2$, $PM_{2.5}$ and HONO, CO and HONO, RH and $HONO/NO_2$ during the entire measurement period, CD, PD, and SPD periods. The blue represented the full measurement period; the light blue represented CD period; the black represented PD period; the red represented SPD period.

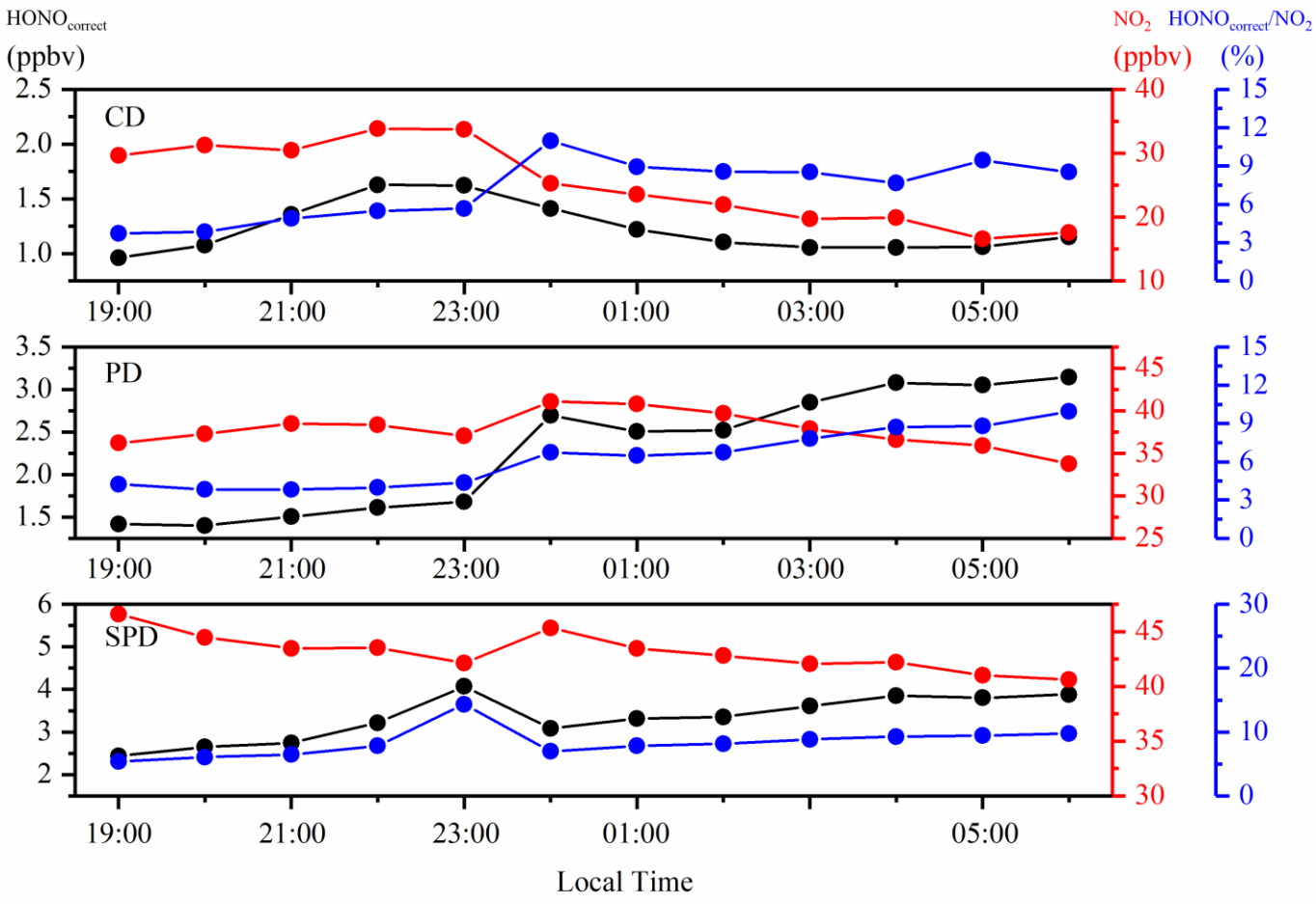

Fig. 8. Nocturnal variations of $HONO_{correct}$, NO_2, and $HONO_{correct}/NO_2$ in CD, PD and SPD periods.

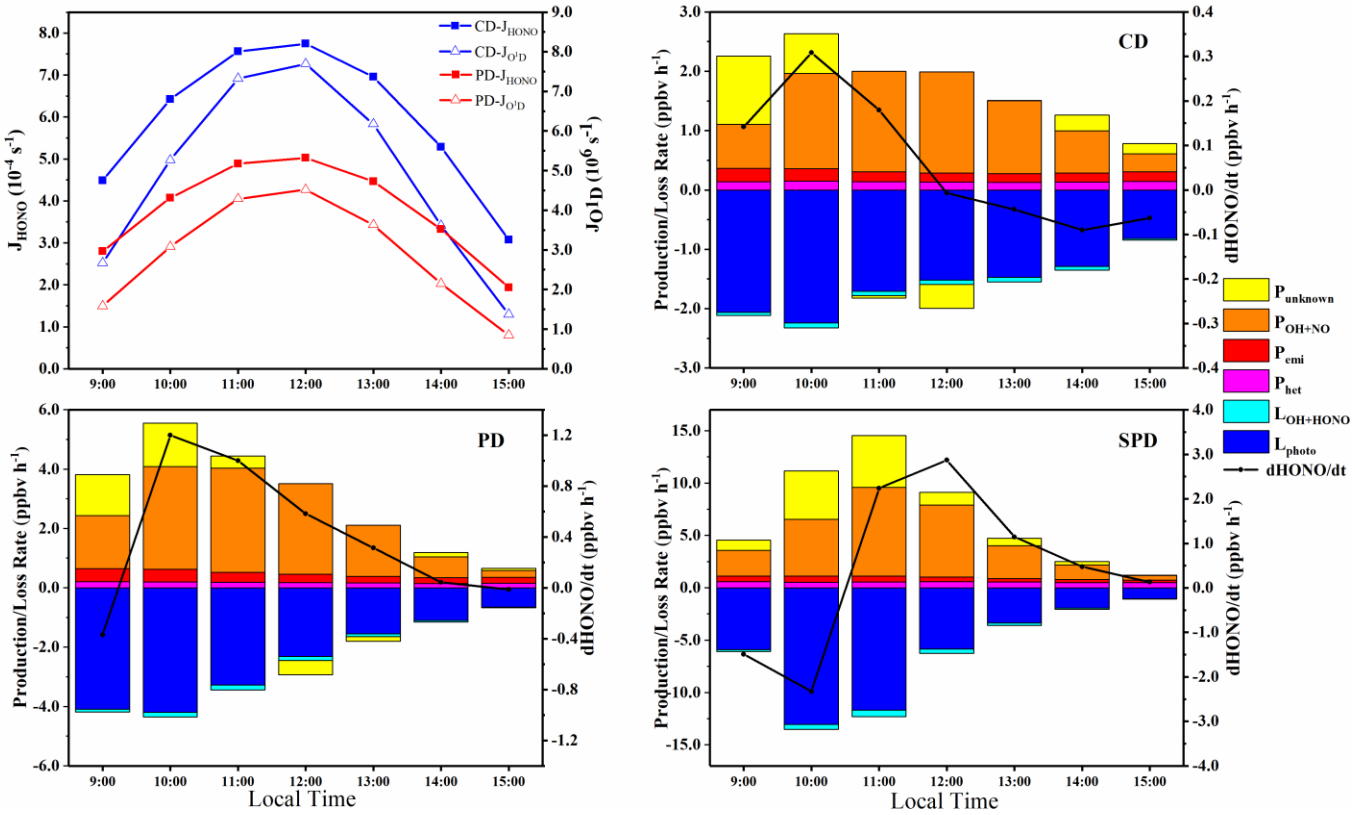

Fig. 9. The average profiles of J_{HONO} and J_{O^1D} concentrations during the daytime, and production and loss rate of the daytime HONO in CD, PD and SPD periods.

Table Captions:

Table 1. Data statistics of HONO, $PM_{2.5}$, NO_2, NO, NO_X, HONO/NO_2, HONO/NO_X, O_3, CO, T, RH, and WS during the measurement period, mean value ± standard deviation.

Table 2. Comparisons of the daytime and nighttime HONO level, HONO/NO_2, and HONO/NO_X mean values in Zhengzhou and other sites around the world.

Table 1.

Data statistics of HONO, $PM_{2.5}$, NO_2, NO, NO_X, $HONO/NO_2$, $HONO/NO_X$, O_3, CO, T, RH, and WS during the measurement period, mean value ± standard deviation.

Trace gases	CD			PD			SPD			Total days
	Day	Night	All	Day	Night	All	Day	Night	All	
$PM_{2.5}$ ($\mu g\ m^{-3}$)	37 ± 15	41 ± 17	39 ± 16	80 ± 32	93 ± 46	87 ± 40	148 ± 29	147 ± 33	147 ± 31	91 ± 54
HONO (ppbv)	0.9 ± 0.7	1.4 ± 0.7	1.1 ± 0.7	1.9 ± 1.7	2.7 ± 1.3	2.3 ± 1.5	3.5 ± 2.7	4.0 ± 1.1	3.7 ± 2.1	2.5 ± 1.9
CO (ppmv)	1 ± 0.3	1 ± 0.3	1 ± 0.3	1± 0.4	1 ± 0.6	1 ± 0.5	2 ± 0.6	2 ± 0.4	2 ± 0.5	1 ± 0.6
NO (ppbv)	18.4 ± 39.3	15 ± 34.3	16.7 ± 36.8	20.3 ± 26.2	30.7 ± 33.6	25.5 ± 30.4	40.8 ± 50.8	64.3 ± 82.1	52.5 ± 68.9	31.8 ± 51.4
NO_2 (ppbv)	23 ± 13	26 ± 13	25 ± 13	29 ± 9	38 ± 10	33 ± 11	40 ± 11	43 ± 10	42 ± 11	33 ± 14
O_3 (ppbv)	21.4 ± 11.5	13.8 ± 10.0	17.6 ± 11.4	17.4 ± 11.9	8.9 ± 8.1	13.1 ± 10.9	15.6 ± 14.2	7.9 ± 7.1	11.8 ± 11.8	14.2 ± 11.7
$HONO/NO_2$ (%)	4.2 ± 3.6	5.3 ± 2.2	4.7 ± 3.1	6.8 ± 5.8	7.4 ± 3.9	7.1 ± 4.9	9.0 ± 7.7	9.8 ± 5.8	9.4 ± 6.8	7.6 ± 6.4
$HONO/NO_X$ (%)	3.3 ± 2.7	6.0 ± 5.6	4.5 ± 4.5	4.4 ± 2.5	4.6 ± 1.7	4.5 ± 2.1	5.3 ± 3.4	5.8 ± 4.7	5.6 ± 4.1	4.9 ± 3.8
RH (%)	30 ± 21	36 ± 20	33 ± 21	44 ± 17	54 ± 18	49 ± 18	64 ± 18	73 ± 13	68 ± 16	50 ± 24
WS ($m\ s^{-1}$)	0.8 ± 1.0	0.5 ± 0.7	0.7 ± 0.9	1.1 ± 1.4	0.6 ± 0.9	0.9 ± 1.2	0.4 ± 0.7	0.3 ± 0.6	0.4 ± 0.7	0.6 ± 0.9
T (°C)	4.3 ± 4.6	2.7 ± 3.6	3.5 ± 4.2	3.7 ± 3.3	2.6 ± 3.1	3.1 ± 3.2	4.6 ± 3.2	2.9 ± 2.1	3.8 ± 2.8	3.5 ± 3.5

Table 2.

Comparisons of the daytime and nighttime HONO level, $HONO/NO_2$, and $HONO/NO_X$ mean values in Zhengzhou and other sites around the world.

Date (Site)	Instrument	HONO (ppbv)			$HONO/NO_2$ (%)		$HONO/NO_X$ (%)		Reference
		Day	Night	N/D	Day	Night	Day	Night	
Oct.–Nov. 2014 (Beijing, urban)	LOPAP (long path absorption photometer)	0.9	1.8	2.0	2.6	4.6	1.7	2.2	Tong et al., 2015
Feb.–Mar. 2014 (Beijing, urban)	LOPAP	1.8	2.1	1.2	3.8 (Severe haze)	4.3	2.5	2.5	Hou et al., 2016
		0.5	0.9	1.8	7.8 (Clean)	3.0	5.1	2.4	
Jul. 2006 (Guangzhou, rural)	LOPAP	0.2	0.9	4.5	1.0	2.5	4.3	4.5	Li et al., 2012
Jul. 2014–Aug. 2015 (Xi'an, urban)	LOPAP	0.5	1.6	3.2	3.3	6.2			Huang et al., 2017
Aug. 2010–Jun. 2012 (Shanghai, urban)	Active DOAS	0.8	1.1	1.4	4.2	4.5			Wang et al., 2013
Jul. 2009 (Paris, urban)	wet chemical derivatization technique-HPLC/UV-VIS detection	0.1	0.2	2.0	3.3	2.5			Michoud et al., 2014
Jan. 2019	AIM	2.2	2.8	1.3	6.8	8.5	4.4	5.5	This study